

General Disclaimer

One or more of the Following Statements may affect this Document

- This document has been reproduced from the best copy furnished by the organizational source. It is being released in the interest of making available as much information as possible.
- This document may contain data, which exceeds the sheet parameters. It was furnished in this condition by the organizational source and is the best copy available.
- This document may contain tone-on-tone or color graphs, charts and/or pictures, which have been reproduced in black and white.
- This document is paginated as submitted by the original source.
- Portions of this document are not fully legible due to the historical nature of some of the material. However, it is the best reproduction available from the original submission.



Flow Visualization and Interpretation of Visualization Data for Deflected Thrust V/STOL Nozzles

(NASA-TM-83554) FLOW VISUALIZATION AND
INTERPRETATION OF VISUALIZATION DATA FOR
DEFLECTED THRUST V/STOL NOZZLES (NASA) 51 p
HC A04/MF A01

N84-14147

CSCS 21E

Unclas

G3/C7 42E16

H. C. Kao, P. L. Burstadt,
and A. L. Johns
*Lewis Research Center
Cleveland, Ohio*

Prepared for the
Twenty-second Aerospace Sciences Meeting
sponsored by the American Institute of Aeronautics and Astronautics
Reno, Nevada, January 9-12, 1984

NASA

FLOW VISUALIZATION AND INTERPRETATION OF VISUALIZATION DATA FOR DEFLECTED THRUST V/STOL NOZZLES

H. C. Kao, P. L. Burstadt, and A. L. Johns
National Aeronautics and Space Administration
Lewis Research Center
Cleveland, Ohio 44135

SUMMARY

Flow visualization studies were made for four deflected thrust nozzle models at subsonic speeds. Based on topological rules and the assumption that observed streaks constitute continuous vector fields, available visualization pictures are interpreted and flow patterns on interior surfaces of the nozzles are synthesized. In particular, three-dimensional flow structure and separations are discussed. From the synthesized patterns, the overall features of the flow field in a given nozzle can be approximately perceived.

INTRODUCTION

Flow visualization has played an important role in fluid dynamics and is still an essential part of many experiments. In fact, more emphasis is being placed upon it now than ever before due to the fact that more complex flows associated with complex geometries are being investigated. At present we depend mainly upon observations to understand the complexity of these flows, since techniques for numerical computations are still under development and not yet sufficiently matured. In addition to the qualitative information that flow visualization traditionally provides, quantitative information may now be obtained, without a laborious effort, from the imaging and numerical processing of flow visualization pictures (ref. 1 for example).

It is well known that interpretation of flow visualization data is a difficult task, due in part to the problems of insufficient resolution and flow separation. Although separation in steady two-dimensional flows is fairly well understood, comprehension of three-dimensional separated flows remains difficult. As a result, potentially useful information sometimes remains in raw data form and undiscovered. Some of these difficulties may now be mitigated by the topological classification of observed singular points. This approach has been applied successfully to external flows in the past few years. The purpose of this report is, therefore, to demonstrate the use of these concepts in internal flows and to present the interpreted results from flow visualization studies for deflected thrust nozzles. Although some of these interpretations constitute still a conjecture, a recourse to topological classifications and rules offers a more rational approach.

If no flow separation occurs and visualization data are reasonably complete, it is not difficult to give an appropriate interpretation. However, since flow separations are commonly encountered in nature as well as in man-made devices, we are often more interested in separated flows than smooth ones. Unfortunately, interpretation of flow visualization data for these flows that frequently involve three-dimensional separations is difficult and has unrelentingly been a controversial subject. At present it appears that the commonly

ORIGINAL PAGE IS OF POOR QUALITY

accepted method is to abandon the use of limiting streamlines and Maskell's model in favor of the notion of skin-friction lines and topological concepts. An early discussion of this topic can be found in a Lighthill's article (ref. 2), but the recent impetus seems to have begun with the presentation by Hunt et al. at the 14th I.U.T.A.M. Congress in Delft, 1976 and their subsequent paper in 1978 (ref. 3). Subsequently, extensive applications to external flows have been undertaken by Tobak and Peake (refs. 4 to 6).

A brief discussion of topological concepts and singularities will be made below. Before proceeding, however, it is perhaps worth noting the advantages and limitations of using topological concepts.

TOPOLOGICAL NOTIONS, RULES AND SINGULARITIES

Advantage and Limitation

The advantage is mainly that through the introduction of topology one can translate physical phenomena, such as stagnation, separation and reattachment points, into mathematical notions that have an accepted meaning in topology. When this is done, one could then apply the existing equations to deduce flow patterns from visualization data.

In fluid mechanics we are used to thinking of local properties, since the governing equations are in the form of partial differential equations and one does not know the global property of a fluid system unless the solutions to these equations are known. Consequently, if visualization data on one part of the surface are not available or do not have sufficient resolution, one cannot, in general, use fluid dynamic means to extend the constructed flow pattern from one area with available data to another area without available data, especially when the latter involves flow separation. This situation is further aggravated by the fact that photographs for separated regions frequently are somewhat blurred, and one is liable to miss important features if flow separations are not accurately delineated, for its existence alone would generally have a dominant effect on the performance of a system. Some of these difficulties could, however, be alleviated by the introduction of simple topological rules, which provide a more rigorous treatment of separation and attachment points and, moreover, are concerned with global rather than local properties.

In delineating flow visualization data the fundamental rules in fluid mechanics are always kept in mind. For instance, a streamline will not be permitted to terminate in the flow field nor will a vortex line be permitted to begin or end abruptly. With the availability of topological concepts another item is added to the list of concepts that avoid implausibilities.

Finally it is noted that the topological rules used here are kinematic and not dynamic for no consideration is given to the influence of pressure and viscous forces. As a result, the flow pattern so constructed represents a kinematically plausible pattern; it may or may not be dynamically acceptable. Nonetheless, it is still considered to be a minimum requirement.

The flow patterns resulting from using oil-film or paint-dot techniques are essentially a multitude of streaks on the surface of a model. The directions of these streaks can be shown to represent closely the directions of skin-friction lines, if the flow visualization indicator is sufficiently thin (ref. 7). On the basis of this assertion, it is assumed that the observed streaks constitute a continuous vector field in which there exists a unique direction associated with every point except at a finite number of isolated points where the shear stress is zero. At these points the skin-friction lines may converge, diverge or coil. These are the singular points which may be classified mathematically into two main types - nodes and saddles. A nodal or saddle point may characterize a stagnation, separation or attachment point in accordance with the direction and property of shear stress in the vicinity of this point. Moreover, each singular point possesses an index which is 1 for a node and -1 for a saddle. The sum of the indices of all singularities on the entire surface of the model is governed by a topological rule. This rule is the Euler characteristic and is invariant for topologically equivalent surfaces. These items will be discussed briefly in the following. For more details, one is referred to refs. 2 to 6 and 8 to 11.

A limiting streamline is commonly defined as the limiting direction of a streamline as the surface is approached. The direction of this line can be shown to coincide with the direction of the skin-friction line in the absence of flow separation. However, as the flow separation is encountered, limiting streamlines must leave the surface as demonstrated in reference 2, whereas the skin-friction lines remain defined and have continuous directions except at singular points.

From the examples of singular points shown in figure 1, it is noticed that the common property of these points is that the continuity of directions breaks down. In particular, a node is a point common to an infinite number of skin-friction lines, where all skin-friction lines except the pair AA are tangent to the pair BB. The node in figure 1(a) where all skin-friction lines converge to the origin, represents a separation point from which a single streamline may depart. If the directions are reversed and skin-friction lines diverge from the origin as shown in figure 1(b), it then has the characteristic of an attachment point. The commonly depicted flow patterns for the forward and backward stagnation point on a sphere, where streamlines are rays emanating from or ending at the stagnation point, are the special cases of a node.

A coiled node or a focus is also a node and has the index of 1 but it has no common tangent line and all skin-friction lines approach the origin on a spiral path as in figure 1(c). This represents generally a separation point from which surface vortex lines may depart and extend into the flow field to form a vortex tube.

Finally a saddle point as given in figure 1(d) has the index of -1 and consists of four rays AA and BB issuing from and terminating at the origin; all of the other skin-friction lines miss the origin and are curves asymptotic to these rays. As a rule this point exists between two nodes. The pair of rays AA in this case act as a barrier to prevent two sets of skin-friction lines from two adjacent nodal points from running into each other. Furthermore, as skin-friction lines approach AA asymptotically, the height of the

ORIGINAL PAGE IS
OF POOR QUALITY

limiting streamlines along this line must increase and hence it is a separation line (ref. 2). A saddle point with or without coiled nodes is often considered to be an essential mechanism for flow to separate, although some questions have been raised recently about this (ref. 12).

The topological rules which we will use are invariant for topologically equivalent surfaces. Surfaces that appear geometrically to be completely different may actually be topologically equivalent, because an elastic deformation in topology is permissible. Thus, for example, with stretching and bending a tetrahedron, a cube and a cone are all equivalent to a sphere. It follows that the same topological rule governing the surface flow patterns of a sphere applies to each of these configurations.

Topological Rules

Since the previous work concerns mainly external flows, the topological rules for these flows may not be applied directly for internal flows. For this reason, we state these rules in the following that will be referred to later.

(a) Skin-friction lines on an isolated body equivalent to a sphere:

$$\sum_n + \sum_s = 2 \quad (1)$$

(b) Skin-friction lines on the interior surface of a torus:

$$\sum_n + \sum_s = 2 - 2g \quad (2)$$

where $g = 1$ for a one-fold torus (donut-like shape) and $g = 2$ for a two-fold torus (donut with two holes)

(c) Streamlines in cross sections of a duct:

$$\sum_n + \sum_s + \frac{1}{2} (\sum_{n'} + \sum_{s'}) = 2 - g \quad (3)$$

where $g = 1$ with no centerbody (simply connected) and $g = 2$ with one centerbody (doubly connected).

(d) Skin-friction lines on the duct surface with two ends open and a porthole:

$$\sum_n + \sum_s + \frac{1}{2} (\sum_{n'} + \sum_{s'}) = -1 \quad (4)$$

(e) Streamlines in planes cutting longitudinally through a duct:

$$\sum_n + \sum_s + \frac{1}{2} (\sum_{n'} + \sum_{s'}) = 1 - g \quad (5)$$

where $g = 1$ with no centerbody and $g = 2$ with one centerbody.

In these equations the symbol \sum_n denotes the sum of indices for node points and the symbol \sum_s the sum of indices for saddle points. In equations (3) to (5) the symbols $\sum_{n'}$ and $\sum_{s'}$ are also used. Here the subscripts n' and s' denote the half node and half saddle respectively found on the boundaries of these configurations. Notice that equations (3) and (5) are for streamlines in planes cutting through a duct transversely or longitudinally.

Equation (1) was considered by Davey and Lighthill (refs. 13 and 2) and equation (2) is a generalization of equation (1). Equations (3) and (4) are special for our purpose and perhaps not to be found in the cited references. Thus, we include a derivation of equation (3) in appendix A. We note here that a hollow cylinder with both ends open is topologically equivalent to an annulus (a disk with a hole). Therefore, the duct with two ends open and a porthole on the surface is equivalent to a disk with two holes, and equation (4) is an extension of equation (3).

These and similar rules have been applied by various investigators to interpret flow patterns observed in experiment or obtained in computation. See, for example, references 3 to 6, and 14 to 15.

Power of Resolution and Simplification of Geometry

The question of resolution seems to arise constantly in almost every visualization study. The power of resolution never seems to be enough; we in fact observe merely the large-scale phenomena. The consequence of this is, therefore, the nonperception of singularities contained in fine structures or the erroneous identification of isolated singularities which, in fact, are clusters of singular points. To what extent will this affect the applications of these rules? Hunt et al. seem to state that as long as the truncated flow patterns are reasonable and continuous, neglect of fine structures may not impair the validity of the interpreted results.

In a similar vein the question whether a model tested in a wind tunnel is an isolated body can be raised. If the model is installed on a sting which, in turn, is attached to the tunnel wall, the combination of the model and sting is actually a part of the wind tunnel, which is transformable to a cylinder or a torus and is not equivalent to, say, a sphere. Nonetheless, equation (1) is still used in such cases. The justification appears to be that the presence of the sting and its attachment to the wall will not significantly affect the flow pattern in the front portion of the model. Similarly, a deflected thrust nozzle may have a fan, turning vanes, core flow entrance or struts. These devices will all affect the flow field to some extent, but since they are upstream of the test section we assume that their influence is small and may be neglected. Thus, when we apply equations (1) to (5) to actual problems no consideration is given to these devices.

TEST APPARATUS AND PROCEDURE

The propulsion systems proposed for medium speed (subsonic) V/STOL aircraft can be categorized as either "fixed nacelle" or "tilt nacelle" systems. When vertical thrust is produced by tilting the nacelle, inlet aerodynamics

ORIGINAL PAGE IS
OF POOR QUALITY

are a primary concern. However, when the nacelle is fixed, aerodynamics of the thrust deflecting nozzle are a principal topic of study. Four fixed nacelle, medium speed, V/STOL aircraft concepts are shown in figure 2. Fixed nacelle V/STOL aircraft require propulsion system nozzles which can provide high thrust coefficients and efficient flow turning over a wide range of operating conditions. This paper presents flow visualization data and interpreted results of the four deflected thrust nozzle concepts utilized by the propulsion systems shown in figure 3. For other aspects of experimental results such as nozzle performance and exit velocity surveys, one is referred to reference 16. These exhaust systems are designed to operate at the low pressure ratios typical of the high bypass turbofan engines most suited for subsonic V/STOL aircraft.

These four configurations are representative of the broad range that have been proposed. Models shown in figure 4 were designed for testing a 30.5 cm (12 in.) diameter fan and an independently controlled core engine flow simulator.

Referring to figure 4(a), the 'D'-vented nozzle configuration consists of a fixed hood, two rotating hoods, a venting lip, and a core nozzle. The fixed hood is an asymmetric contoured component in which the fan duct transitions from the circular annulus just ahead of the nozzle entrance station, to a 'D' shaped cross section. In the deflecting mode the flow turning process for both fan and core flow is completed in the 'D'-shaped rotating hoods.

The chin nozzle system consists of a contoured centerbody, cowl, cascade vane (chin) nozzle, and aft nozzle as shown in figure 4(b). Part of the fan airflow is deflected downward, through the cascade vanes. The remainder of the airflow is discharged further aft. This model hardware was designed to study the chin nozzle performance and flow field, and the centerbody represents the turbofan core engine. The hardware aft of the cascade is used simply to remove part of the fan airflow.

The split-flow flap nozzle system shown in figure 4(c) consists of both a front and an aft deflecting nozzle for fan airflow. This system has a separate nozzle for core engine flow. At some operating conditions almost 100 percent of the fan flow is deflected through the front nozzle.

The tandem-fan front nozzle of figure 4(d) consists of an S-duct nozzle and a fairing to cover the base of the fan hub. Both the nozzle wall and the fairing transition vary rapidly from circular to rectangular cross-sections. The lower wall of the S-duct is a two-piece hinged flap, which is rotated to deflect the nozzle flow for V/STOL operation. This nozzle uses only fan airflow.

The photo in figure 5 shows the 'D'-vented nozzle installed on the Vertical Thrust Stand at the NASA Lewis Research Center. An inlet bellmouth supplied air to a 30.5 cm (12 in.) diameter fan, which was driven by a tip turbine. Concentric ducts for the fan and turbine discharge flow, and an independently controlled core flow, connected the fan and the nozzle. The nozzle exhausted upward, past the remotely controlled exit flow survey rake. Figure 6 illustrates the internal ducting arrangement and the location of the rake used to measure nozzle entrance conditions. When nozzles which did not require

ORIGINAL PAGE IS
OF POOR QUALITY

core airflow (figs. 4(c) and (d)) were tested, the core nozzle shroud was replaced with an appropriate closed fairing.

The flow patterns inside the nozzles were visualized by means of a streak-line technique. Artist's oil paint was mixed with a lightweight oil to control viscosity. The best results were obtained when the viscosity of the mixture was just low enough so that a drop would maintain its shape when placed on a vertical surface. A pattern of dots was applied to the internal surfaces of the nozzle using hypodermic syringes. Colors were selected and arranged in an attempt to provide streak-lines in the regions of interest. The streak-lines were generated by quickly opening the control valve to establish the desired nozzle flow conditions within about 3 to 5 sec, and then maintaining that flow rate for an additional 5 to 10 sec. The development of the streak-lines was observed via closed circuit television. Although the paint and oil mixture began to flow during the start-up procedure, the streaks began to develop in a direction that was consistent with the final pattern. Most of the final pattern developed at the desired operating condition and no change was observed during the shutdown procedure. Flow visualization results were recorded on 35 mm color film using a hand-held camera, and on color video tape.

RESULTS AND DISCUSSION

D-Vented Nozzle

A photograph of this model installed on the test stand is shown in figure 7. In addition to the centerbody, which is not visible in this photograph but can be seen in figure 8, there is a fairly thick side-force plate (yaw vane) attached to the nozzle wall along the centerline of the vent lip. The deflection of the nozzle begins somewhere in the trailing region of the centerbody. Since the nozzle was designed to deflect both the fan and the simulated engine core flow, there is also a duct for the core flow. This duct terminates somewhat upstream of the bend. However, in order to reduce the problem to a manageable level, we make the following simplifications about geometry: (a) The centerbody is an isolated body of finite length; the effect of thin struts is small and negligible. (b) The presence of the core flow duct is neglected, as the core flow was either turned off or matched with the fan flow with the same static pressure when visualization studies were made. With these two simplifications, the vented nozzle becomes essentially a pipe bend with an isolated centerbody and a side-force plate attached to the wall.

Cross-Sectional Streamline Patterns

As this is a curved nozzle with a bend angle in the range of 110° , occurrence of secondary flows is expected. Their appearance should become noticeable shortly after entering the bend. The secondary flow in a curved pipe without the centerbody is usually represented by two vortices if viewed cross-sectionally. These are actually spiral motions in the bend. The development of the secondary flow is commonly explained on the basis of unequal pressure distributions induced by the centrifugal force, but it may also be explained by the transport of vortex lines as given in reference 17. In accordance with the latter argument, we now expect to see four vortices in the bend when viewed cross-sectionally, the reason being that there are two vortex rings of

opposite sense prior to the bend (one in the boundary layer of the pipe wall and the other in the boundary layer of the centerbody) and the transport of these through convection results in streamwise vorticity that, in turn, induces the secondary flows as indicated schematically in figure 9. This figure has 4 nodes (foci), 2 saddles and 4 half saddles, which satisfies equation (3) with $g = 2$. It suffices to say that this condition will not be met if the secondary flow has only 2 cells.

Further downstream in the trailing region of the centerbody, it is envisioned that as the centerbody reduces its diameter and finally disappears, the inner cells tend to coalesce and become smaller in size. As a result, the vortices are more concentrated and intensified. The two spiral nodes in figure 8 are likely to be the foci where the fluid coiled and emanated from the inner pair of vortical cores. (This is not a good picture to show the foci on the centerbody. It is chosen because it shows the position of the centerbody relative to the venting lip and side-force plate.) Since the centerbody here bears some resemblance to the blunt slender bodies tested by Peake et al., it is expected to find some similarity between these two cases. However, by observing the skin-friction line patterns in figures 27 and 28 of reference 5, no evidence is seen that flow separates in a similar manner. In particular, the two spiral nodes in the trailing region, which are so apparent in figure 8, were absent there. Thus, it is thought that the secondary flows in our case substantially changed the flow behavior over a blunt slender body.

The sketches shown in figure 10 are our interpretation of figure 8. There is a node point of attachment in figure 10(a) which, we think, should probably be there, although it was not observed in any available photographs. Because of its presence, two adjacent saddle points have to be added. If this node point is absent, the synthesized pattern may become figure 10(b). In fact, this is all one can confidently see in visualization pictures.

The combination of a pair of foci and a saddle point as in figure 10 represents a known mechanism that the flow leaves the surface in the form of a "wake". At this stage the two outer vortical cores of the secondary flow should still exist but may have been displaced upward. Thus, the cross-sectional streamline pattern looks probably like the one sketched in figure 11. Note that this is a simply connected region and the condition of equation (3) with $g = 1$ is met.

This proposed streamline pattern is only valid in the distance between the centerbody and the side-force plate. When the latter is encountered, the arrangement of streamlines must adjust accordingly to accommodate its presence. The modified streamline pattern is sketched approximately in figure 12. The pair of half-saddles on the upper part of the side-force plate represents the projection of a pair of attachment lines, that are fairly visible in figure 13. The two spiral cells embracing the side-force plate are essentially the original two inner vortical cores. There are two segments of free boundary produced by the venting lip, and two local separation zones on the hood due to the unevenness of the junction. Note that this is still a simply connected region since the side-force plate is attached to the nozzle wall.

Streamlines in Plane of Symmetry

In order to present a more complete picture of the D-vented nozzle flow field, it is perhaps useful to sketch a streamline pattern in the plane of symmetry as shown in figure 14. When an obstacle is placed on a surface facing an incoming flow, the surface boundary layer will, in general, interact with the obstacle to create a horseshoe vortex wrapping around the obstacle. In the present case the side-force plate is placed immediately downstream of the venting lip. As the wall stress is suddenly removed from the stream the flow must adjust itself. Consequently, another shear layer will develop to satisfy the condition of zero stress at the free surface. This shear layer is, however, very thin initially, since it must also rely on diffusion to increase its thickness. For this reason, it is assumed that only the original boundary layer is capable of inducing horseshoe vortices. Although there is only one horseshoe vortex depicted in the present problem, it is possible to have several horseshoe vortices all induced by the same boundary layer flow.

This horseshoe vortex does not, in general, contact the obstacle directly and there is often a small local separation region between these two as shown in figure 14. Similarly there is a local separation zone at the bottom of the side-force plate. The presence of the former cannot be verified since no paint dot was applied in that region, while the presence of the latter may be inferred from the dab of paint in the corner (fig. 13). The half-saddle on the leading edge of the side-force plate is the stagnation point from which the streamlines emanate, skirt around the side and move inward on the bottom of the plate. The streak in figure 13 seems to indicate this inward motion.

The centerbody is depicted here as an isolated body and the distribution of singularities is based on figure 10(b). If the finer structure is included as in figure 10(a), there will be more singular points on the surface including a node due to the appearance of reattachment. Note that this is a doubly connected region and equation (5) is applicable.

In summary, it is envisioned that in a short distance after entering the bend the flow developed spiral motions consisting of two pairs of vortical cores; these vortices interacted with the centerbody and the side-force plate resulting in a fairly complex flow field including the separation at the centerbody, the horseshoe vortex and the local separation on the side-force plate. The secondary flow at the exit viewed cross-sectionally contained two pairs of vortices originally generated by the nozzle bend but altered through interactions.

Chin Nozzle Model

Two photographs are included in figure 15 to show the exterior and interior of the experimental chin nozzle model. It consists of mainly a duct, a centerbody, and a front nozzle with cascade vanes. During its performance tests, many variations of the geometry were made. These variations were essentially concerned with the angle, shape, opening and closing of cascade vanes; the basic configuration remained unchanged. Although each of these variations induced some change in performance data, the basic flow pattern, especially in the areas away from cascades, did not appear to vary. For this reason, the patterns synthesized in the following are mainly based on one set

of skin-friction lines. No attempt is made to identify what constitutes the best performance.

Geometry and Simplification

As with the D-vented nozzle the centerbody is fastened to the nozzle wall by thin struts. Based on the similar argument, we assume that the effect of these struts is small and may be neglected. Thus, the centerbody becomes an isolated body. We further assume that the front nozzle is essentially a porthole without cascade vanes. The inner surface of the simplified geometry as sketched in figure 16 without the centerbody is then topologically equivalent to a triply connected disk (disk with two holes) for which equation (4) is applicable. It seems that this simplification is essential, for otherwise the nozzle with n cascade vanes will be equivalent to a $(n + 3)$ -tuply connected disk and a high resolution of visualization will be required to perceive details of the flow on and around these vanes. With this simplification the constructed flow pattern would be somewhat similar to a picture observed by a distant observer in which details are lost but gross features are preserved.

Rendition of Flow Patterns on Nozzle Interior Surface

The rendition of skin-friction lines on the nozzle interior surface is mainly based on two photographs shown in figure 17. These pictures were taken at two different angles for the area near the cascade exit (porthole exit). The cascades and centerbody were present in the experiment but were removed when these photographs were taken.

The disposition of skin-friction lines interpreted from figure 17 is sketched in figure 18 on a triply connected disk, which is actually fairly similar to the projection of the nozzle as seen in figure 17. We notice that in this figure surface streamlines (skin-friction lines) enter the front nozzle mainly through four corners where they converge. Thus, there are a number of singular points on the rim of the porthole. In addition, there is a saddle point on the plane of symmetry between the front and aft nozzle where two dividing streamlines meet. The fluid on one side of this line exits through the front nozzle, while that on the other side through the aft nozzle. There is no evidence that the flow is separated on the nozzle interior surface, although separations take place on the centerbody.

Rendition of Flow Patterns on the Centerbody

Because a large proportion of the fan flow (up to 80 percent) may depart from the front cascade vanes, the centerbody often experiences a strong lateral flow. This environment is somewhat similar to that of a slender body in a stream at a high angle of attack. It is known that under this condition flow usually separates at the leeward side. It is thus expected to encounter a similar situation for the centerbody. The large spiral nodes in figures 19 and 23 attest to the possibility of sizable flow separation. Although there is an analogue between the present case and a slender body, there are differences. A slender body in a uniform stream experiences the effect of angle-of-attack everywhere, whereas it is limited to the forward section in the present

case. Thus, the flow pattern in the forward and aft sections are rather different.

The interpretation of the skin-friction lines in figure 19 is shown in figure 21. We postulate that there are three stagnation points on the centerbody: two are the familiar ones at the nose and tail region and the third one is on the windward side in the waist region. As a result, there exists at least one saddle point on the windward side. From this point two separation lines originate, which encircle the body and eventually enter the foci. In addition, there are two attachment lines emanating from the stagnation point on the windward side. These can be seen in figure 19(b) where skin-friction lines diverge, which are perhaps also the dividing streamline. The vorticity created in the boundary layer forward of this line spirals into the foci to form the two vortical cores and eventually leaves the surface in a swirling "wake".

In order to perceive the presence of this wake, we installed a plate on the plane of symmetry for flow visualization as shown in figure 20. With the cascade vanes in place and open, the streaks on the plate are seen to be straight and pointing outward, which means that there is virtually no recirculatory motion in the departing stream. This finding contradicts the observed flow pattern on the centerbody. To explain this inconsistency, we subsequently removed all vanes and took flow visualization pictures as in figure 20(b). The photographed pattern is clearly different and we think that this is caused by the swirling motion of the wake. If we now make a simplification that the wake consists essentially of two counter-rotating helix-like vortices, one of which facing the camera is in the clockwise direction, and assume that the streaks seen on the plate are trajectories of the velocity vectors at the back of this helix, we may then compare figure 22 with figure 20(b). The fact that they are similar seems to imply that cascade vanes effectively suppressed the swirling motion in the present case.

Change of Flow Patterns due to Changes of Cascade Openings

The above discussions and the sketched skin friction lines were essentially based on photographs taken from two experimental runs in which the cascade exit was partially closed four passages open and two closed. When all six passages were open or cascade vanes were removed completely, a noticeable difference was observed in that the symmetric pattern on the centerbody gave way to a nonsymmetric pattern as shown in figure 23. In other words, as the ratio of the fan flow exiting the front nozzle to that through the aft nozzle increases, the flow changes from a symmetric to an asymmetric pattern. This is probably caused by the not entirely symmetric installation of the front nozzle.

The synthesized skin-friction line pattern for this case is given in figure 24. The main features of this pattern on the leeward surface are based on the photographs such as the ones in figure 23. The finer structures are added in accordance with equation (1) and the rule that a saddle point cannot be connected directly to another saddle point. If this rule is relaxed, the main features remain the same but there are fewer secondary separation lines. The pattern at the windward surface is essentially a modification of the symmetric pattern in figure 21. It is not an interpretation of the observation,

CHARACTERIZATION OF FLOW

because the windward side of the body was not well photographed. It is expected that both pairs of vortical cores on the leeward side leave the surface. However, since the middle two cores are very close together and the strengths are weaker, it is possible that they may coalesce and disappear from the scene shortly after leaving the surface. Finally, in view of the fact that the flow is asymmetric about the geometric plane of symmetry on the centerbody, it is likely that it is asymmetric everywhere in the nozzle.

In summary our perception of the flow field in the chin nozzle model is as follows. There was a dividing surface in the nozzle which divided the entering fluid into two parts. The part exhausting through the front nozzle caused a fairly severe flow separation in the leeward side of the centerbody, while the other part exhausting through the aft nozzle was essentially smooth. In addition, as the ratio of exhaustion through the front nozzle to that through the aft nozzle increased above a certain limit, the flow on the centerbody became nonsymmetric. This implies that the flow was probably nonsymmetric everywhere.

Split Flow Nozzle Model

Among the four configurations considered here, the split flow nozzle has the most complex geometry; most of the interior surface is not visible from the outside and hence was not photographed. Figure 25(a) shows basically the front nozzle and the visible part of the interior surface. The split plate (divider) spans the entire nozzle and is very thick with a blunt leading edge, from which the centerbody is attached. Thus, the centerbody is not an isolated body but may be viewed as a protrusion of the divider. The function of the divider is to split the flow into the front and aft nozzle. The plate, which is raised in the photograph, is the so-called cover plate for the front nozzle, and the plate written with the number 39 is the flap. When the cover plate is down and the flap is horizontal, flush with the divider's lower surface (the visible surface in figure 25(a)), since the model was installed inversely, the nozzle is in the cruise mode. When the cover plate is removed and the flap is in the upright position, it is in the deflected thrust mode.

Figure 25(b) shows the aft nozzle and its installation. There are two exits for this nozzle. The lower one is for the engine core flow but was always closed in this experiment. The upper exit is for the fan flow and has two flaps. The position of these flaps determines whether the nozzle is in the cruise or deflected thrust mode.

Tests in this experiment were conducted under three conditions: (i) the cruise mode, (ii) the deflected thrust mode with the front and aft nozzles open and (iii) the deflected thrust mode with the front nozzle alone open. These cases are to be discussed separately in the following.

Geometric Artifice and Simplification

Since the geometry for this model is fairly complex and the flow visualization was never provided on the surfaces which cannot be seen readily from the outside, the synthesis of flow patterns is more speculative than the previous cases. Furthermore, geometric artifices are introduced to facilitate

the applications of topological rules. The purpose is to render the present model into a configuration of known property so that equation (2) can be applied directly.

After neglecting struts and other auxiliary structures and by means of stretching and bending, we may transform the present model into a pipe joint branching out to the front and aft exits. Furthermore, if we connect sections of an imaginary pipe to this transformed nozzle, a two-fold torus may result as sketched in figure 26(a). The turning of the imaginary pipes is assumed to be so gentle that the flow undergoes very slow change and no singularity appears except at the junction labeled A, where a saddle point exists due to the convergence of two streams into one (ref. 3). With a two-fold torus, equation (2) with $g = 2$ is applicable. However, since a saddle point is always present on the surface of imaginary sections the condition for singular points on the actual nozzle surface becomes

$$\sum_n + \sum_s = -1 \quad (6)$$

In the case that the front nozzle alone is open, this reduces to a simple torus indicated in figure 26(b). Now since no singularity is required in the imaginary sections, the condition for the actual nozzle becomes

$$\sum_n + \sum_s = 0 \quad (7)$$

Flow Pattern for Cruise Mode with Both Front and Aft Nozzles Open

Cross-Sectional Streamlines. - As can be seen in figure 25 or 27, the cross section of the nozzle in the entrance region enlarges abruptly within a short distance. This situation is somewhat similar to that of a pipe with an abrupt expansion, for which it is known that the flow will separate and an annular eddy (vortex ring) will usually emerge to regulate the effective area. In the present case since the configuration is not axisymmetric, the flow separation is not expected to be in the form of an annular eddy. Instead it will probably be comprised of four swirling cells; the reason is that in addition to the plane of symmetry there is a divider, which effectively partitions the nozzle into four compartments. The lower pair of swirling cells can be observed, for example, in figure 27(a) but the existence of the upper pair is assumed. The postulated pattern for this is given in figure 28(a). It has 4 nodes and 8 half-saddles to give the difference of zero as required by equation (3) with $g = 2$. The upper pair are probably fairly weak and of limited extent. However, if they are absent, it is difficult to conjure up a reasonable pattern and still to be able to meet the requirement of equation (3).

The acceptance of the assumption that cellular structures are to be found in the entrance region enables us to deduce skin-friction line patterns by proceeding downstream gradually. First a cross-sectional streamline pattern for the front nozzle is, however, sketched. The fact that the streaks on the cover plate (fig. 27(b)) are nearly horizontal indicates that the flow in the lower part of the nozzle is essentially separated with strong swirls. As a result, the effective area of the front nozzle is much reduced. A look at streaks on the cover plate reveals that they converge to two separation lines

ORIGINAL PAGE IS
OF POOR QUALITY

on either side of the centerline, which form a triangular zone with its apex approximately at the exit. The directions of streaks inside the triangle are pointed outward, while those outside the triangle are inward. This information suggests the appearance of two vortices in the lower portion of the nozzle (see fig. 28(b)). These are the same pair of vortices indicated in the lower portion of figure 28(a) but somewhat flattened.

Since the directions of streaks on the flap are mainly axial, a large porportion of the flow is believed to exit through here. The streaks converge sidewise to two corners to form two attachment lines. These lines are represented cross-sectionwise by two half-nodes in the upper corners of figure 28(b). Their presence induces the streamlines to converge to two corners. Hence these are the half-node points of attachment. The condition that streamlines bend downward from the middle, split and then swing upward reflects perhaps the fact that fluid particles have to climb over the divider to head for the exit.

Interior Surface Skin-Friction Lines. - In order to have a more complete picture of the flow, an attempt is made here to supplement these streamline patterns by synthesizing a skin-friction line pattern for the entire interior surface. The difficulty here is the lack of visualization data. Furthermore, since the configuration is complex and three-dimensional, it is not possible to represent the entire surface in a single diagram. Consequently, the pattern has to be excised and portrayed in several pieces. When visualization data are available, the depicted skin-friction lines in these pieces are required to agree with the streaks. When not available, we have to rely mainly on topological rules to supplement the missing information.

To begin with, figure 27(a) has to be interpreted and the pattern on the part of the surface not photographed has to be completed. Notice that the lower edge in this figure is connected with the cover plate through a hinge line. Thus, the streaks on the cover plate are a continuation of those in figure 27(a). We now unfold the entrance region and postulate a skin-friction line pattern as sketched in figure 29. In this figure it is seen that there are four segments of dividing streamlines that are the intersections of the dividing surface with the wall. On one side of this surface the flow exits through the front nozzle and on the other side through the aft nozzle. There are two saddle points along these lines, where the dividing streamlines from the leading edge of the divider and the intake meet. In addition, there is a saddle point at the edge of the intake, which has the appearance of a half-saddle but is actually a complete one. The remaining half is inside the intake duct and hidden. This is illustrated in the insertion with the inside surface partially folded out. Below this saddle is a node point of attachment. Its location is somewhat upstream of the cover plate hinge line and hence is not visible in figure 27(b). Finally it is noted that the points in figure 29 are not necessarily at the same axial station since this is essentially a projection.

To continue we now interpret figure 27(b) to synthesize a skin-friction line pattern for the underside of the centerbody and divider. A close-up view of the centerbody is available and given in figure 30. The dominant feature in these photographs is the absence of streaks in the tip region of the centerbody. Streaks entering from upstream made either a right or left turn to avoid

ORIGINAL PAGE IS
OF POOR QUALITY

this area, whereas those downstream of it tend to diverge sidewise. This indicates the occurrence of a saddle point and a separation zone. Our interpretation of this feature is sketched in figure 31(a). The reason that flow separation occurs on the underside instead of the topside is due to the fact that the front nozzle is larger than the aft nozzle and well over one half of the flow exhausts through the former. Consequently, the centerbody and the divider experience a negative angle-of-attack. This disposition of skin-friction lines agrees with figure 28(b) and bears a close resemblance to one type of flow separation on the leeside of a blunt cone. Thus, figure 31(b) is included here for comparison. Since the flow is mainly separated in the middle of the front nozzle, we expect to find a low energy region there. The measured total pressures in figure 32 confirms this prediction. This completes the discussion of flow patterns on the underside of the divider.

Our attention is now turned to the topside of the divider. The analogue of negative angle-of-attack suggests that all stagnation points have to be on the upper surface of the centerbody and divider. It is assumed that there is one stagnation point on the centerbody and one each on either side of the divider as indicated in figure 33(a). There are also two saddle points between these stagnation points to prevent the skin-friction lines from running into each other. Furthermore, these skin-friction lines split around the saddle points to head for the front or aft nozzle. Some of these are then the segments of the dividing streamlines. In addition, there are two saddle points in figure 33(a) that are not labeled and are the duplicates of the two saddle points along the dividing streamlines in figure 29. These points, though appearing to be at the leading edge, are actually somewhat upstream of it. To illustrate this a projection of a side view in figure 33(b) is included.

Figure 34 shows streaks on one of the surfaces of the aft nozzle. These streaks are all parallel and pointed forward. It is, therefore, assumed that there is no singularity in the aft nozzle. With this assumption the singularities in the entire nozzle can now be counted. There are altogether 11 saddle and 10 node points in figures 29, 31(a) and 33(a), giving the difference of -1 as required by equation (6).

Flow Pattern for Deflected Thrust Mode with 90° Flaps

In the deflected thrust mode the front and aft nozzles are open, the cover plate is removed, and all flaps are set at 90°. Otherwise, conditions were similar to those in the cruise mode. The skin-friction line patterns in the entrance region and at the topside are assumed to be similar also. Thus, figures 29 and 33(a) remain valid. Patterns at the underside of the divider and the aft nozzle are, however, different because of the 90° flaps. These are synthesized in the following.

The visualization picture for the flap and the underside of the front nozzle is shown in figure 35, and the postulated skin-friction line pattern is plotted in figure 36. There are two stagnation points on the flap which are caused by forward moving streams from the entrance region. In addition, there are three saddle points to act as barriers from which segments of the separation line emanate. Due to the disposition of these singular points the skin-friction lines in the hinge line region split mainly into two general directions. The lines with outward directions exit through the flanges of the

ORIGINAL PAGE IS
OF POOR QUALITY

nozzle and those with inward directions converge to the tip of the centerbody to form a node of separation. The low energy flow is, therefore, accumulated mainly in a band around the separation line and the tip of the centerbody.

It is thought that what is postulated here is an over-simplification of the actual flow with a 90° flap. It is known that if an obstacle is placed on a surface in a stream, one or more horseshoe vortices will be generated to embrace the obstacle together with a possible local flow separation region between the horseshoe vortex and the body. The present situation is similar except that the horseshoe vortex is bent upward on two sides. Therefore, finer structures of the flow ought to exist. However, due to the insufficient resolution of the available pictures no attempt is made to include them.

For the aft nozzle we observe that the streaks on the outer flap in figure 37 are straight and nearly parallel, but those on the inner flap show signs of flow separation. We thus assume that there exists no singular point on the outer flap (a stagnation line along the hinge line does not bring about singularities). Furthermore, we propose that there is no singular point on the inner flap upstream of the hinge line, because the flow accelerates initially and will not separate. The flow cannot, however, in general remain attached downstream of the hinge line if the turning is abrupt. In the present case it appears that the flow is attached in the central area but separated on the two sides. Our interpretation of this pattern is shown in figure 38. In this figure the flow reattaches itself after coiling around two node points between two pairs of saddle points. With the disposition of singular points as indicated in figures 29, 33(a), 36, and 38, we obtain the difference of the total number of the nodes and saddles to be -1 as required by equation (6).

Flow Pattern for Deflected Thrust Mode with Aft Nozzle Closed

The experimental setup here was similar to the previous case except that the aft nozzle was now closed and all the fan flow exhausted through the front nozzle. As a result the flow deflection by the flap, though intensified, is still similar. This is quite evident in figure 39 apart from the fact that the node of separation at the tip is replaced by two foci. With the availability of this information and the assumed flow pattern in the interior as in the previous case, it is possible to propose skin friction lines for the entire nozzle satisfying the condition of equation (7). However, due to the similarity of these two cases no sketches are shown here.

In summary it is perceived that the sudden expansion of the nozzle area in the entrance region produced two pairs of vortical cores, of which the lower pair caused the flow to separate severely in the front nozzle at the cruise condition, whereas the upper pair being smaller and weaker was probably sufficiently decayed before reaching the aft nozzle and did not produce a noticeable adverse effect. However, when all flaps were down, separated flows were observed in both front and aft nozzles. The separation in the front nozzle was somewhat like the horseshoe vortex induced by an obstacle and that in the aft nozzle was somewhat similar to the separation in a tight pipe bend.

Tandem-Fan Front Nozzle

As stated earlier the model for the tandem-fan front nozzle consists essentially of an S-duct and a centerbody (fig. 40). The model bears some resemblance to the front nozzle of the split-flow model. The lower surface of the S-duct is roughly equivalent to the cover plate and the upper surface corresponds to the underside of the divider. Thus it is not surprising to see similarities in flow patterns as well. A case in point is shown in figure 41. Comparing this picture with figure 27(b), it is found that streaks on the lower surface all converge to two separation lines on the two sides of the centerline. Though the similarity here is obvious, the cause of flow separation is probably different. In the case with the split-flow nozzle the flow separation is caused by the vortices generated by the expansion of the entrance, while in the present case it is probably induced by the vortices detached from the centerbody. The latter is somewhat analogous to the situation of a D-vented nozzle sketched in figure 9 with the lower surface here corresponding to the outside of the bend. It follows that the flow separation may be reduced if the centerbody is modified to conform better with the stream direction (fig. 40(b)). This turns out to be the case by comparing figure 41 with figure 42.

When the lower wall is rotated to deflect the nozzle flow as shown schematically in figure 40(a), the flow makes a fairly rapid turn to exhaust vertically. However, since the flap here acts as an extension of the bend, no major flow separation pattern was observed in the available photographs, especially when the sharp corner between the nozzle and flap is filled with a filler plate.

CONCLUDING REMARKS

In parallel with measurements for performance coefficients and exit velocity distributions for models of four deflected thrust nozzle concepts, flow visualization studies were made. The obtained visualization pictures enabled us to delineate skin-friction line patterns on the nozzle interior surfaces in accordance with topological rules. Based on the postulated trajectories, the structures of three-dimensional flow separations were discussed and sequences of flow development were assembled. This study demonstrated that an appropriate interpretation of flow visualization data can enhance our understanding of flow properties in inlets and nozzles, especially when complex geometries are involved. A summary of perceived features of the flow field in each of the three models can be found at the end of each section.

APPENDIX A

We assume that a given disk has a number of interior and boundary singular points as shown in figure A-1(a). The latter are regarded as half singularities. A disk can, however, be stretched to form a sphere with a circular porthole as shown in figure A-1(b). This transformed configuration has the same number of singularities with their relative positions unchanged. If there is another disk of the same size as the circular hole and with the same number of singularities as the original disk, including the half-singular points distributed in such a manner that they can be matched with the half singularities around the circular hole to form complete singular points, this disk can then be used to cover the hole to produce a complete sphere without a gap and with all complete singular points. In this case the topological rule for singularities on the complete sphere is known to be

$$\Sigma_n + \Sigma_s = 2$$

Because this sphere contains two sets of the original disk singularities, it is

$$\Sigma_n + \Sigma_s + \frac{1}{2} (\Sigma_{n'} + \Sigma_{s'}) = 1$$

for each set, which is essentially equation (3) with $g = 1$. This method can be generalized to include other cases in equation (3) or (4). Note that the steps taken here in deriving this equation are somewhat similar to those in reference 3.

ORIGINAL PAGE IS
OF POOR QUALITY

REFERENCES

1. Imaichi, K., and Ohmi, K., "Numerical Processing of Flow-Visualization Pictures - Measurement of Two-Dimensional Vortex Flow," Journal of Fluid Mechanics, Vol. 129, Apr. 1983, pp 283-311.
2. Lighthill, M. J., "Attachment and Separation in Three-Dimensional Flows," Laminar Boundary Layers, edited by L. Rosenhead, Oxford Press, London, 1963, pp. 72-76.
3. Hunt, J. C. R., Abell, C. J., Peterka, J. A., and Woo, H., "Kinematical Studies of the Flows around Free or Surface-Mounted Obstacles; Applying Topology to Flow Visualization," Journal of Fluid Mechanics, Vol. 86, May 15, 1978, pp. 179-200.
4. Tobak, M., and Peake, D. J., "Topology of Two-Dimensional and Three-Dimensional Separated Flows," AIAA Paper 79-1480, July 1979.
5. Peake, D. J., and Tobak, M., "Three-Dimensional Interactions and Vortical Flows with Emphasis on High Speeds," NASA TM-81169, 1980.
6. Tobak, M., and Peak, D., "Topology of Three-Dimensional Separated Flows," Annual Review of Fluid Mechanics, Vol. 14, 1982, pp. 61-85.
7. Maltby, R. I., "Flow Visualization in Wind Tunnels Using Indicators," AGARDograph No. 70, 1962.
8. Kaplan, W., "Ordinary Differential Equations," Addison-Wesley Publishing Co., Inc., Reading, Mass., 1958.
9. Flegg, G. H., "From Geometry to Topology," Crane-Russak Co., Inc., New York, 1974.
10. Smith, J. H. B., "Remarks on the Structure of Conical Flow," Progress in Aerospace Sciences, Vol. 12, 1972, pp. 241-272.
11. Perry, A. E., and Fairlie, B. D., "Critical Points in Flow Patterns," Advances in Geophysics, Vol. 18B, 1974, pp. 299-315.
12. Wang, K. C., "On the Disputes about Open Separation in Three Dimensional Flow," AIAA Paper 83-0296, Jan. 1983.
13. Davey, A., "Boundary Layer Flow at a Saddle Point of Attachment," Journal of Fluid Mechanics, Vol. 10, June 1961, pp. 593-610.
14. Kao, H. C., "Some Aspects of Calculating Flows about Three-Dimensional Subsonic Inlets," NASA TM-82789, 1981.
15. Deiwert, G. S., "Topological Analysis of Computed Three-Dimensional Viscous flow Fields," NASA TM-84255, 1982.
16. Burstadt, P. L., and Johns, A. L., "Experimental Results of a Deflected Thrust V/SIOL Nozzle Research Program, NASA TM 83069, 1983.

17. Agrawal, Y., Talbot, L. and Gong, K., "Laser Anemometer Study of Flow Development in Curved Circular Pipes," Journal of Fluid Mechanics, Vol. 85, April 13, 1978, pp. 497-518.

ORIGINAL PAGE IS
OF POOR QUALITY

ORIGINAL PAGE IS
OF POOR QUALITY

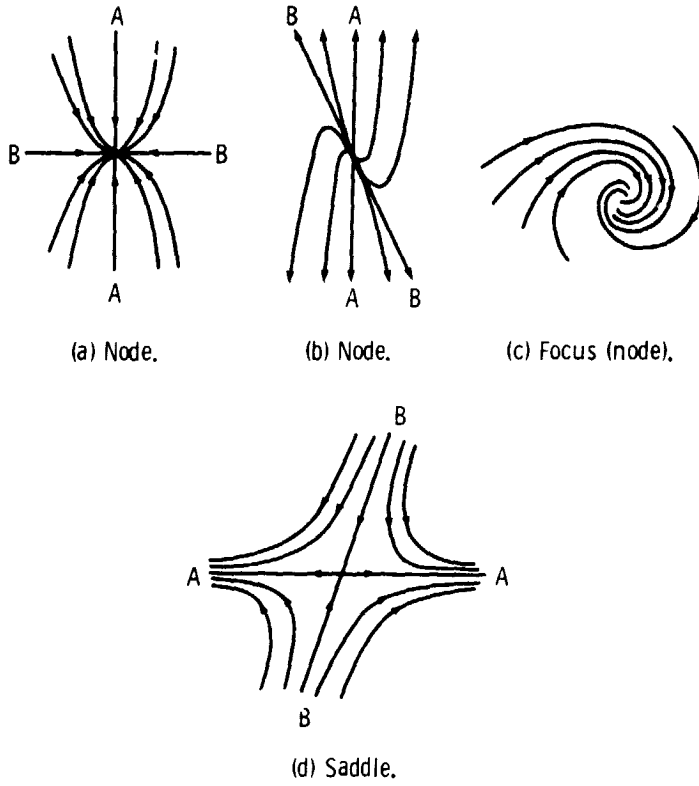
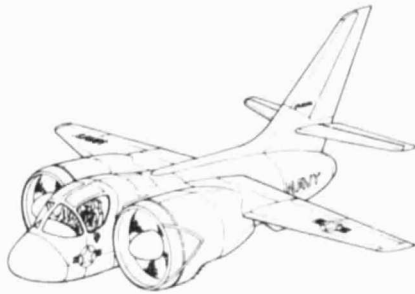
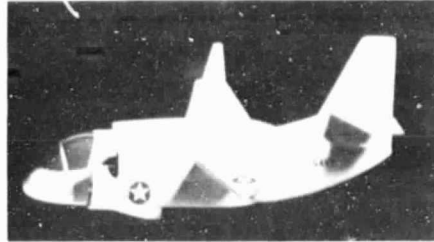
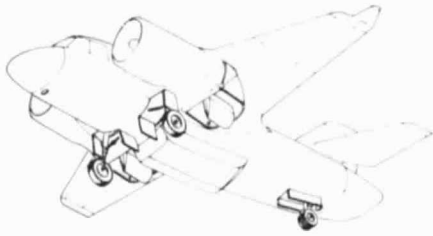


Figure 1. - Examples of nodes and a saddle.

ORIGINAL PAGE IS
OF POOR QUALITY



CS-82-3584

Figure 2. - Medium speed VISTOL aircraft concepts.

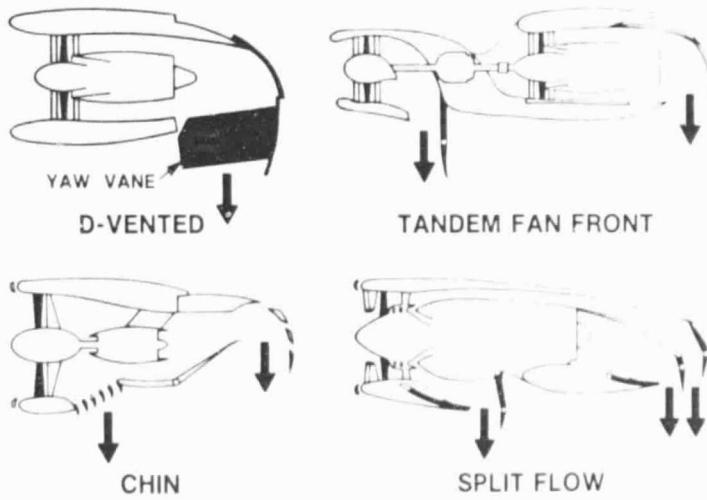
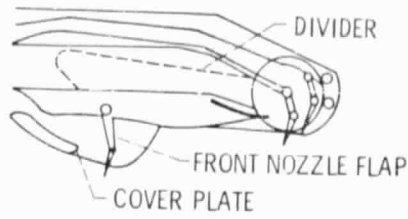


Figure 3. - Medium speed VISTOL propulsion concepts.

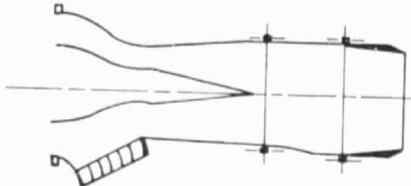
ORIGINAL MODELS
OF POOR QUALITY



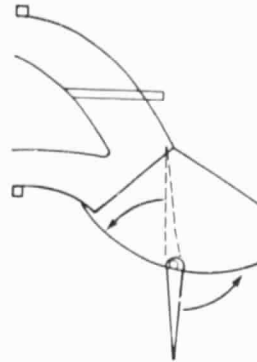
(a) 'D'-vented (with-
out yaw vane).



(c) Split flow flap system.



(b) Chin cascade split flow system.



(d) Tandem-fan front.

Figure 4. - Experimental models.

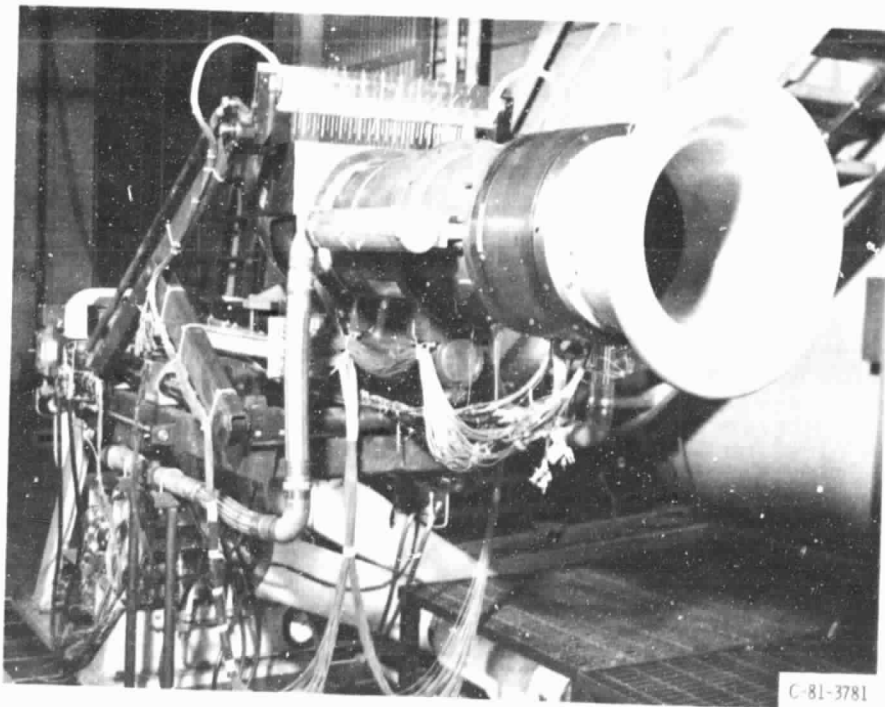


Figure 5. - Test installation with 'D'-vented nozzle and survey rake.

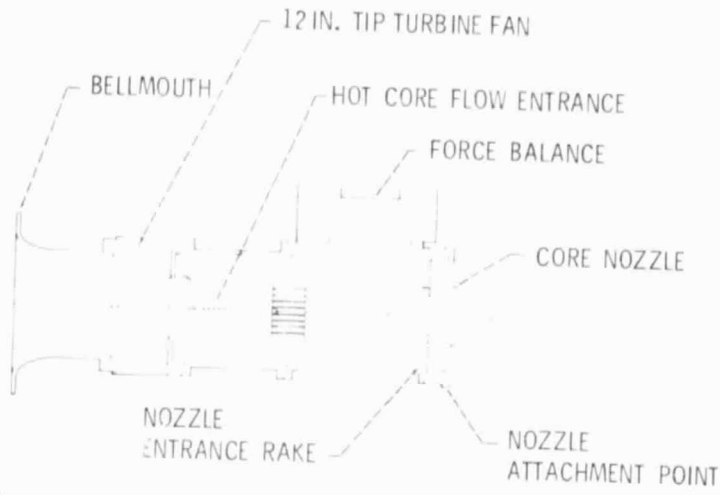


Figure 6. - Schematic of hardware to provide air to test nozzles.

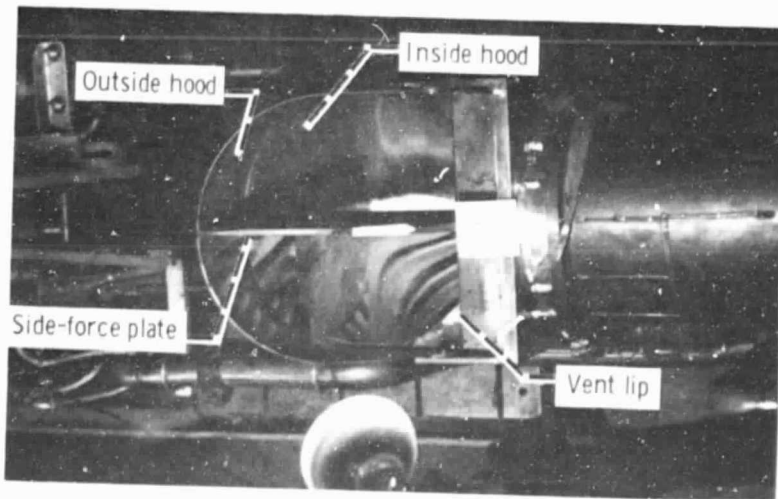


Figure 7. - D-Vented nozzle experimental model.

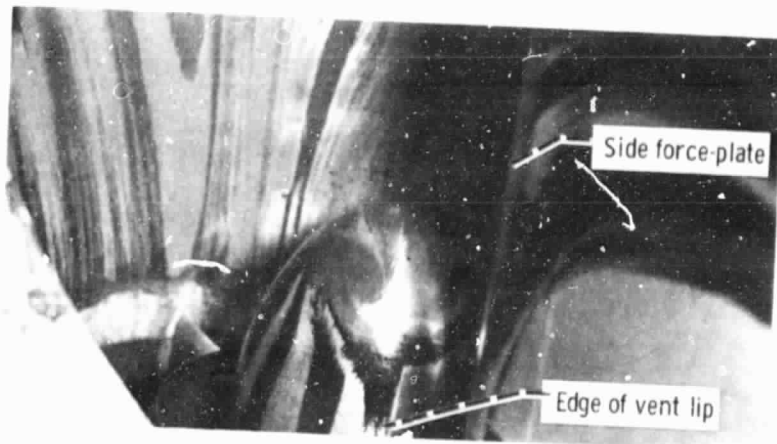


Figure 8. - Streaks on centerbody.

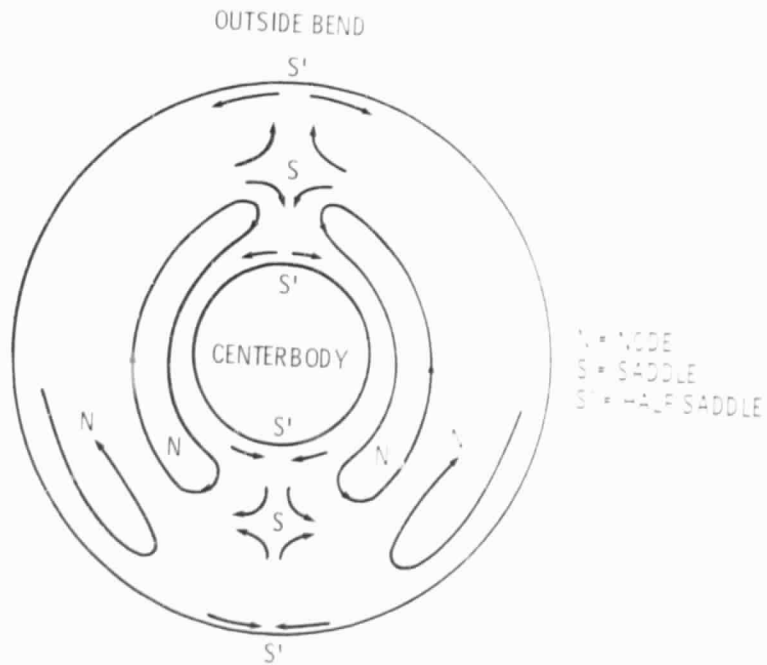


Figure 9. - Postulated cross-sectional streamline pattern shortly after the beginning of bend.

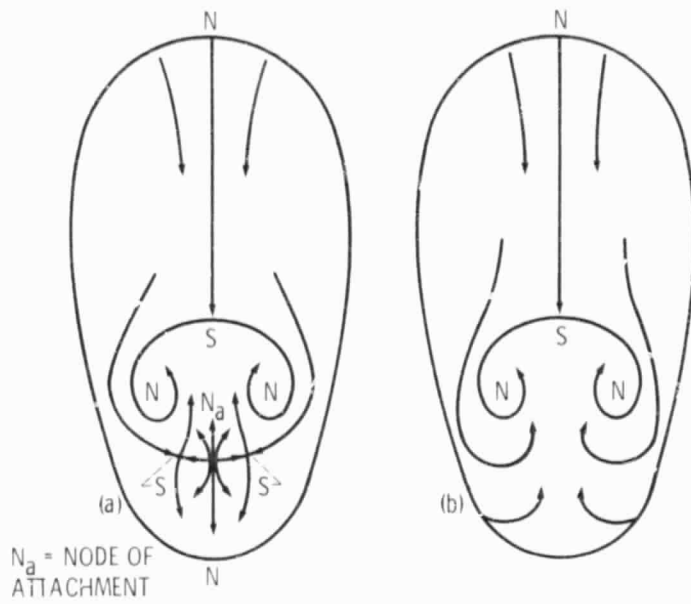


Figure 10. - Postulated skin-friction lines on Leeward side of centerbody.

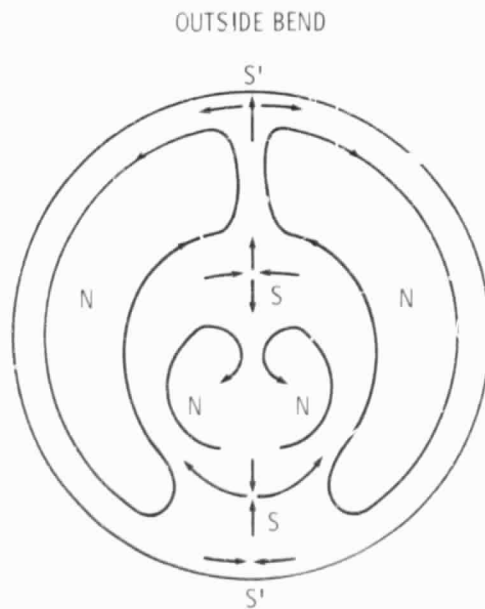


Figure 11. - Plausible cross-sectional streamlines immediately downstream of centerbody.

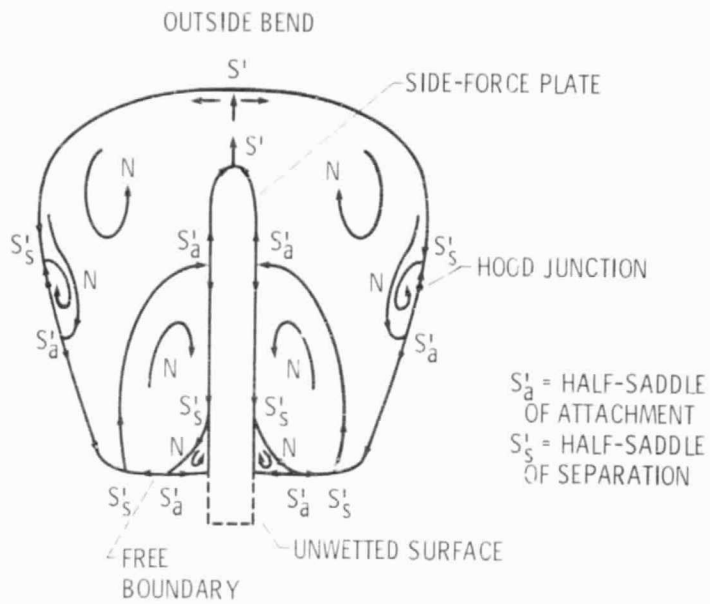


Figure 12. - Postulated cross-sectional streamlines with side-force plate.

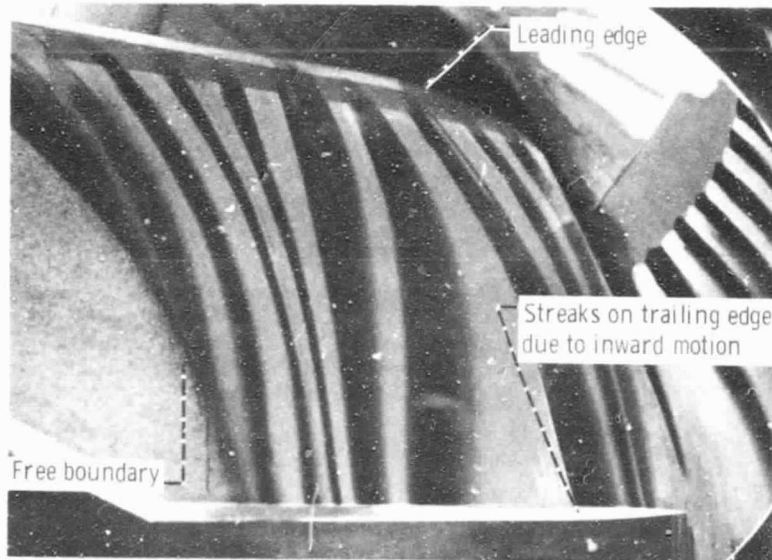


Figure 13. - Photograph of streaks on side-force plate.

ORIGINAL PAGE IS
OF POOR QUALITY.

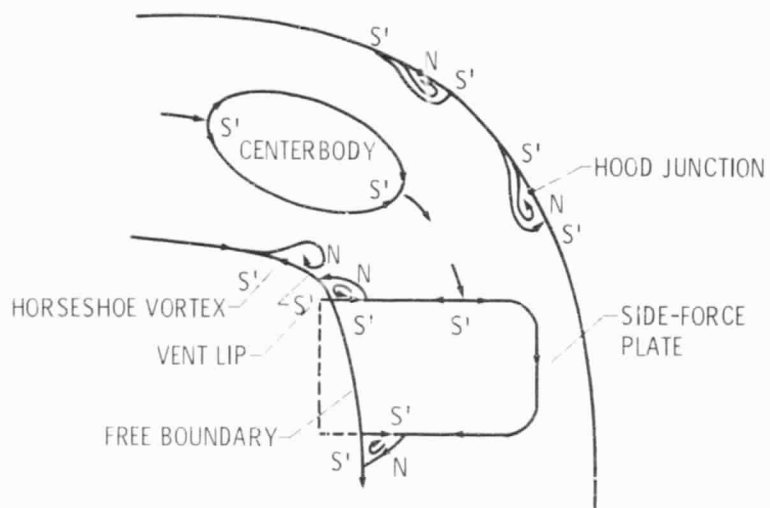


Figure 14. - Postulated flow pattern in plane of symmetry of a D-vented nozzle.

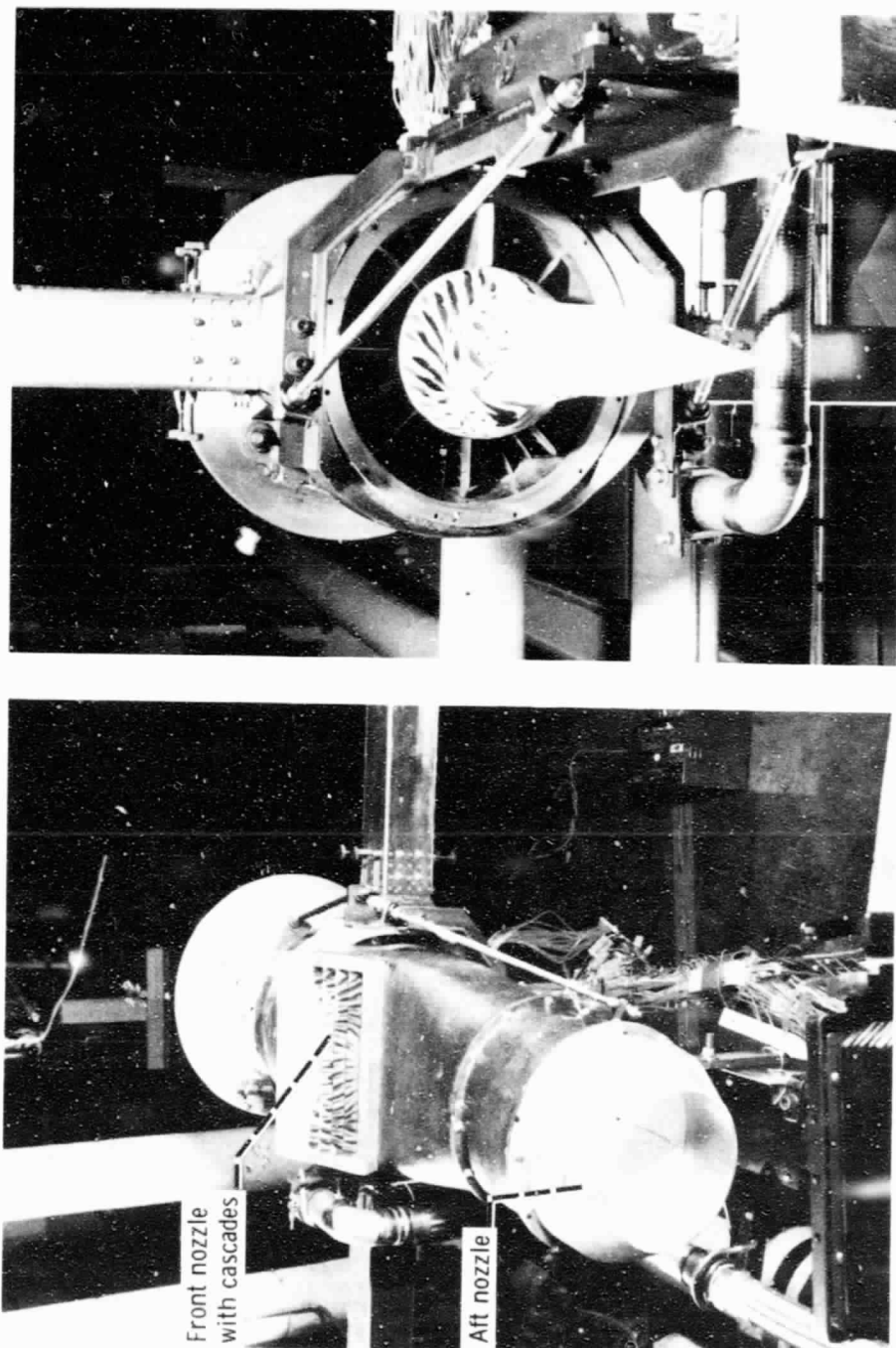


Figure 15. - Two views of chin nozzle model.

ORIGINAL PAGE IS
OF POOR QUALITY

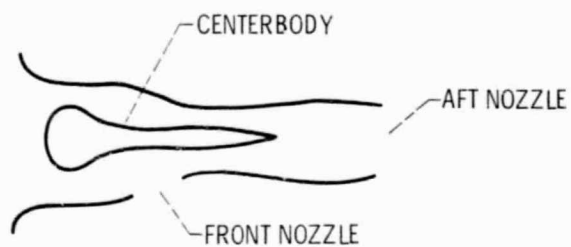


Figure 16. - Simplified chin nozzle model.

ORIGINAL PAGE IS
OF POOR QUALITY

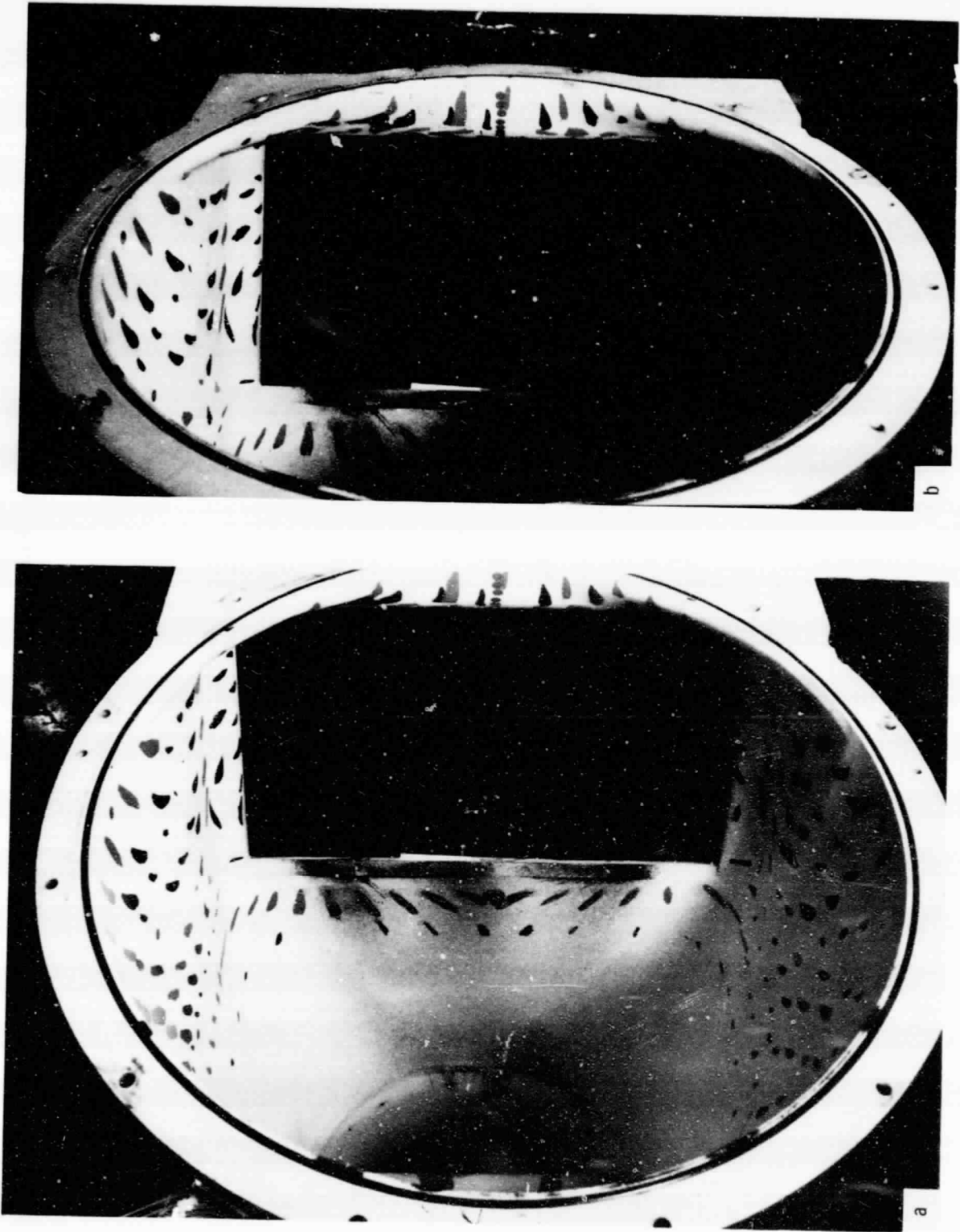


Figure 17. - Photographed streaks on nozzle interior surface.

ORIGINAL PAGE IS
OF POOR QUALITY

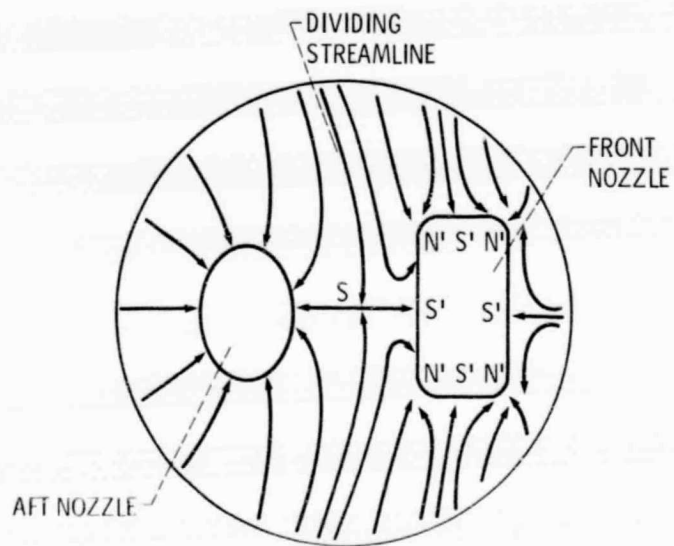
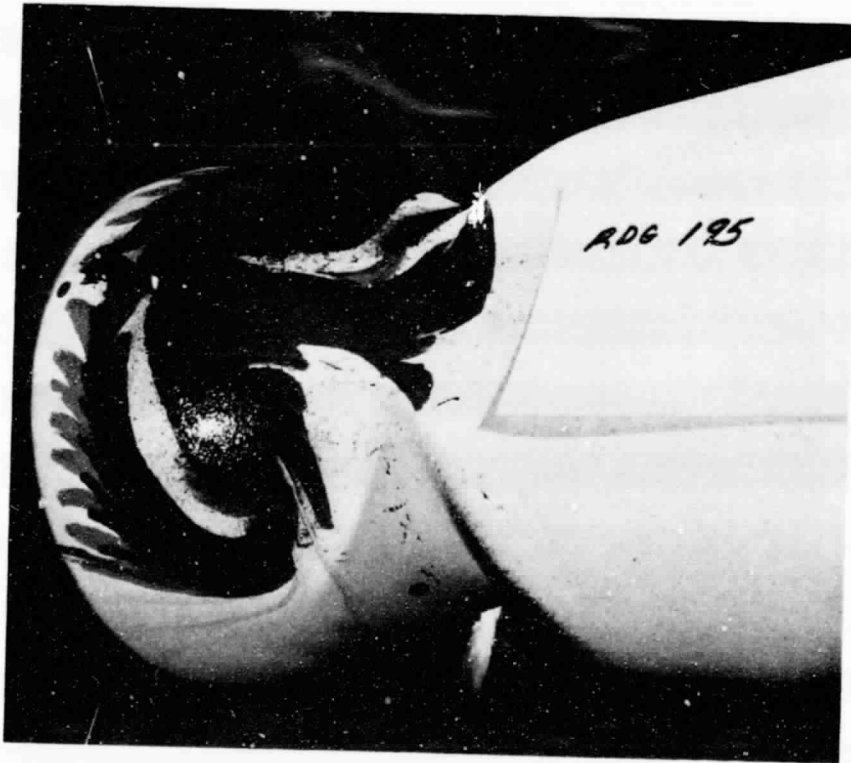


Figure 18. - Postulated skin-friction lines on nozzle interior surface.

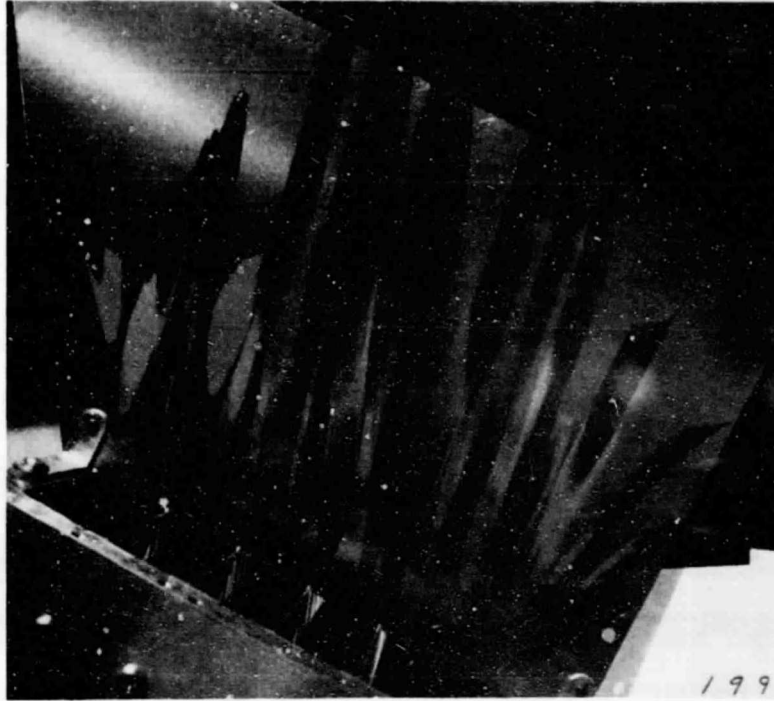


(b) Partial windward side.



(a) Leeward side.

Figure 19. - Patterns of streaks on chin nozzle centerbody.



(a) Cascade vanes open.



(b) Cascade vanes removed.

Figure 20. - Photographed streaks on visualization plate.

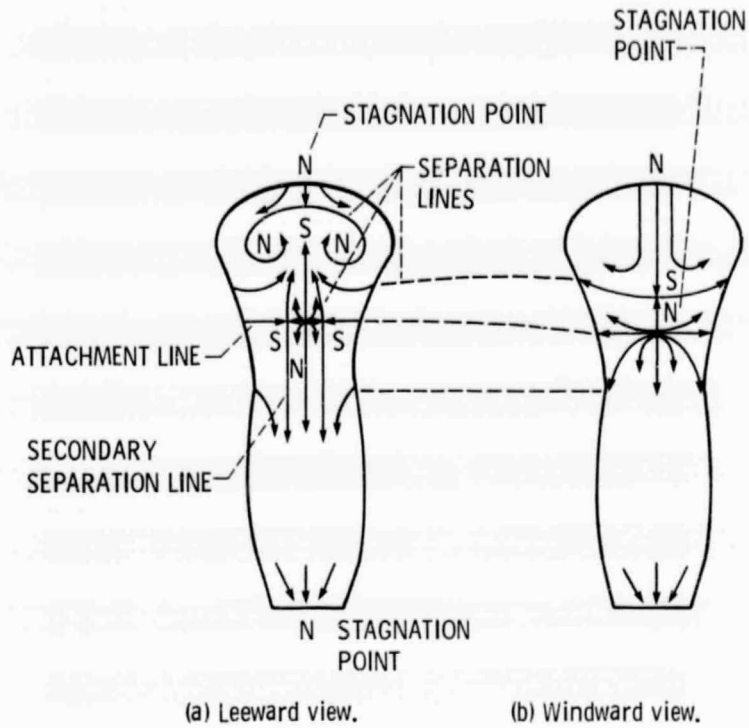


Figure 21. - Postulated skin-friction lines on chin nozzle centerbody with 4 cascade vanes open.

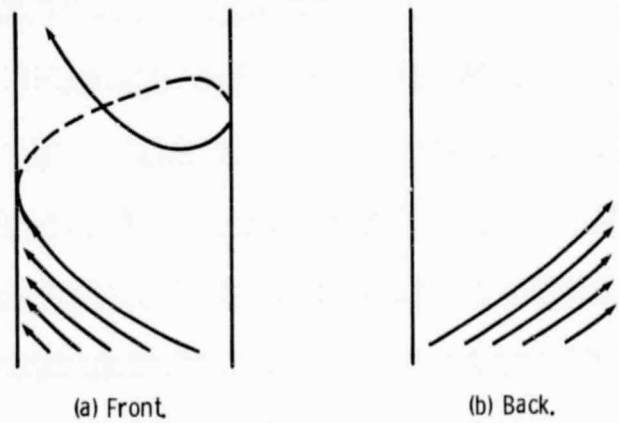


Figure 22. - Projected velocity vectors of a clockwise helix.

ORIGINAL PAGE IS
OF POOR QUALITY



(a) Leeward side.



(b) Partial windward side.

Figure 23. - Ströms on centerbody with cascades fully opened.

ORIGINAL PAGE IS
OF POOR QUALITY

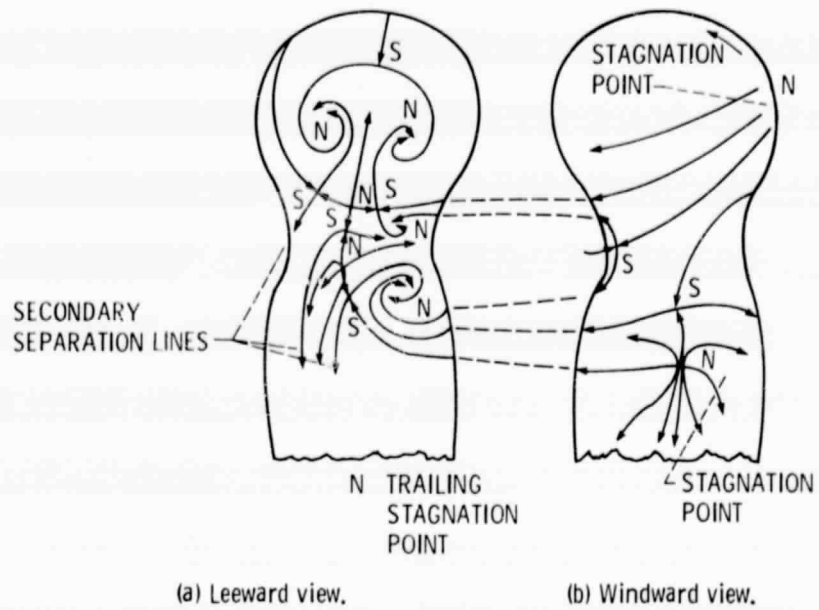
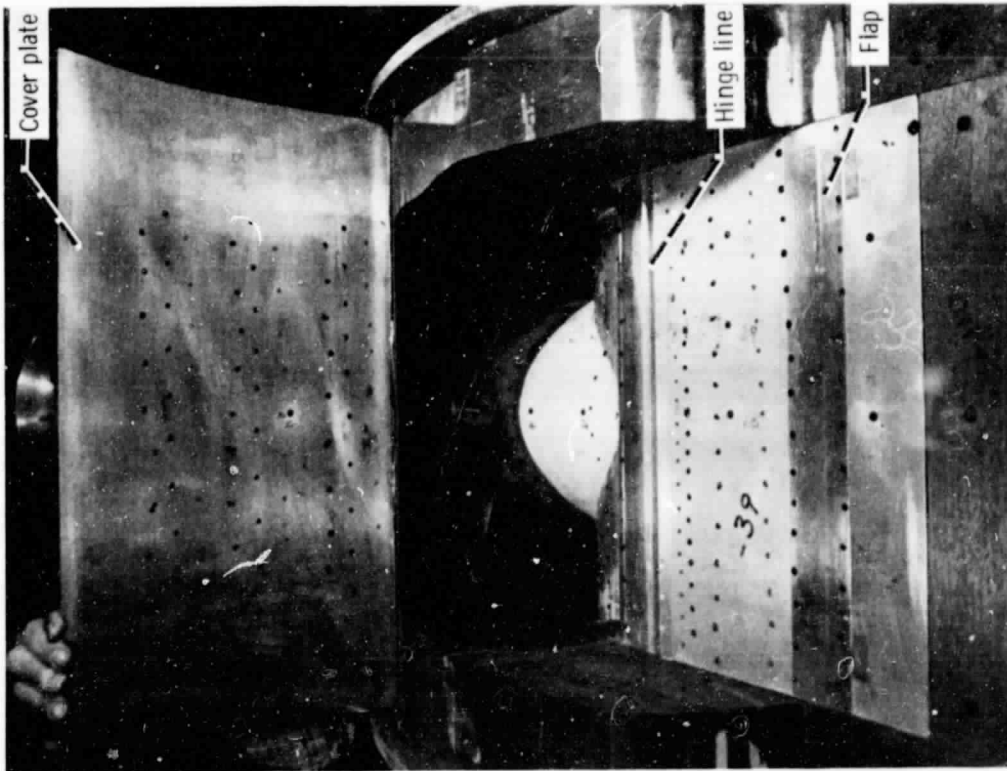
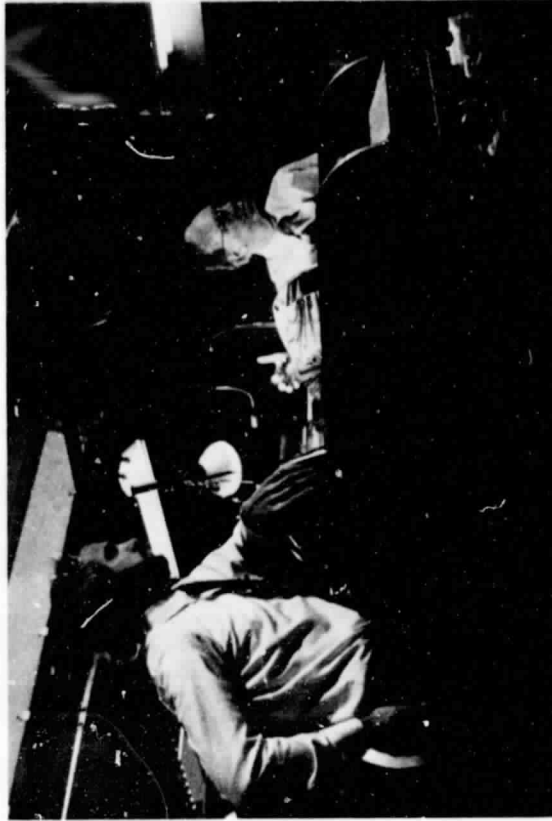


Figure 24. - Synthesized skin-friction lines on chin nozzle centerbody
with cascade vanes fully opened or removed.

ORIGINAL PAGE IS
OF POOR QUALITY



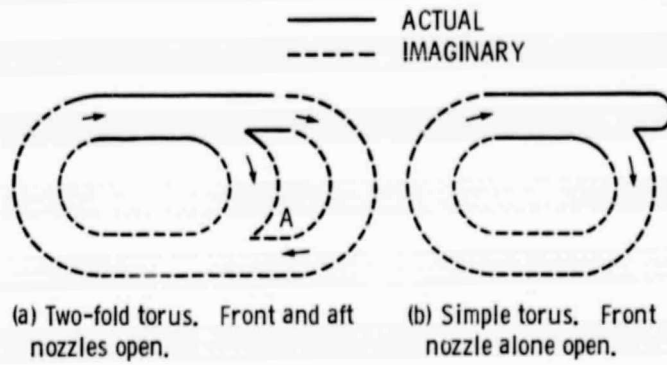
(a) Front nozzle and interior.



(b) Aft nozzle.

Figure 25. - Split flow nozzle model (installed inversely).

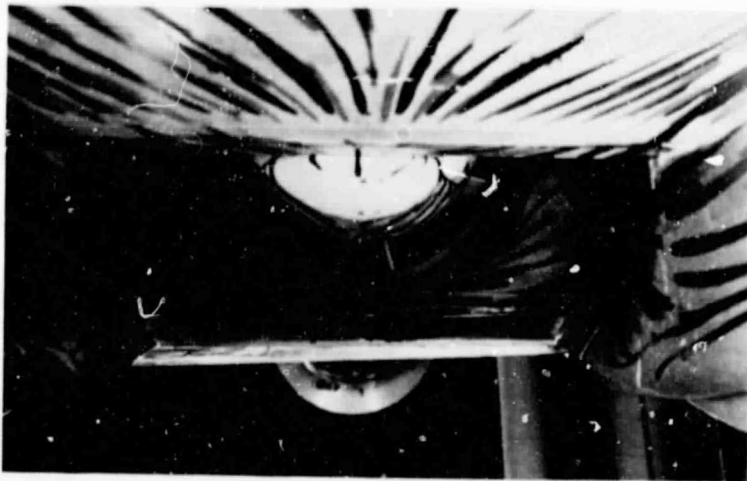
ORIGINAL PAGE 16
OF POOR QUALITY



(a) Two-fold torus. Front and aft nozzles open.

(b) Simple torus. Front nozzle alone open.

Figure 26. - Transformed nozzles after connecting imaginary pipes.



(a) Cover plate removed.

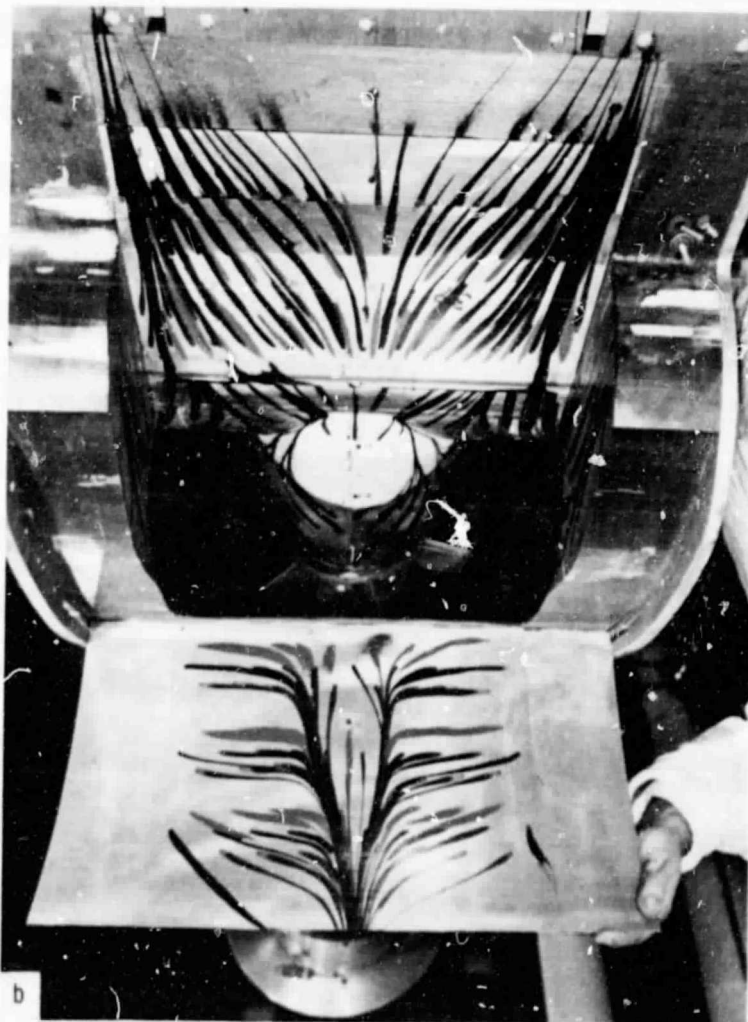
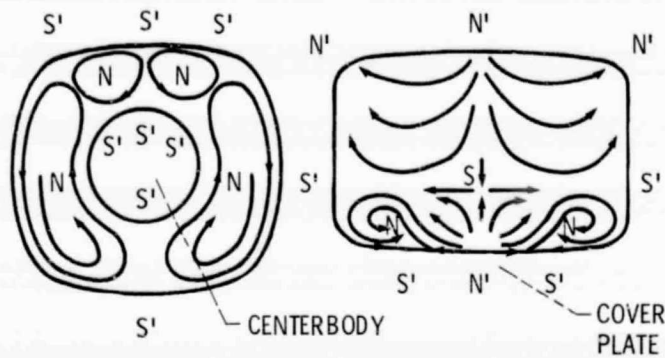


Figure 27. - Flow visualization on surfaces of front nozzle.



(a) Nozzle entrance region.

(b) Front nozzle.

Figure 28. - Cross-sectional streamline patterns at entrance and front nozzle.

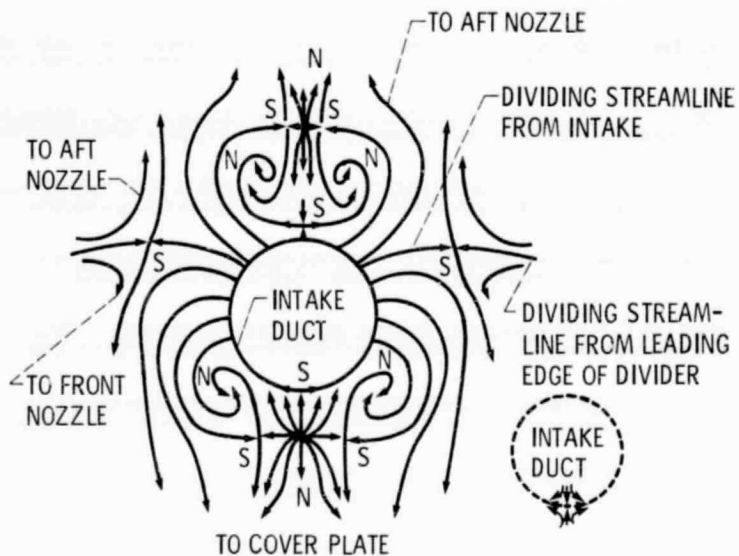
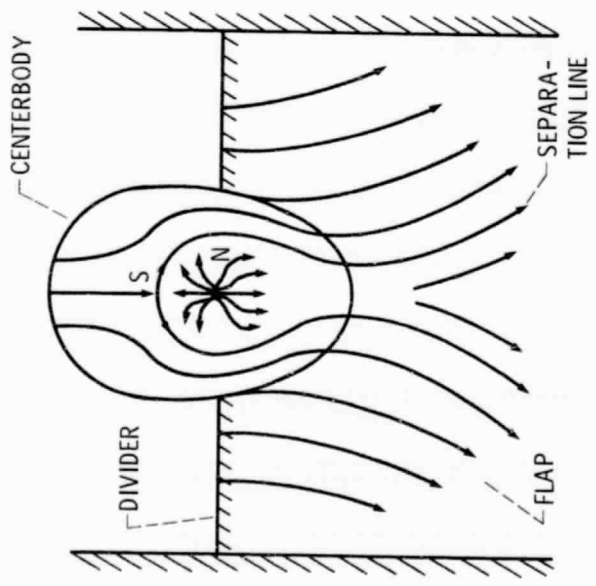


Figure 29. - Postulated skin-friction lines in entrance region of a split flow nozzle.

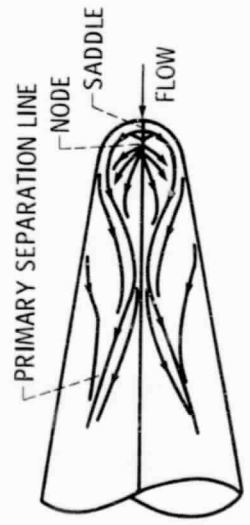
ORIGINAL PAGE IS
OF POOR QUALITY



Figure 30. - Close-up view of centerbody's underside.



(a) Underside of divider and centerbody.



(b) Leeside of blunt cone. (Reproduced from Peake and Tobak, Ref. 5.)

CONTOUR LABEL	CONTOUR VALUE
A	0.750
B	.775
C	.800
D	.825
E	.850
F	.875
G	.900
H	.925
I	.950
J	.975
K	1.000

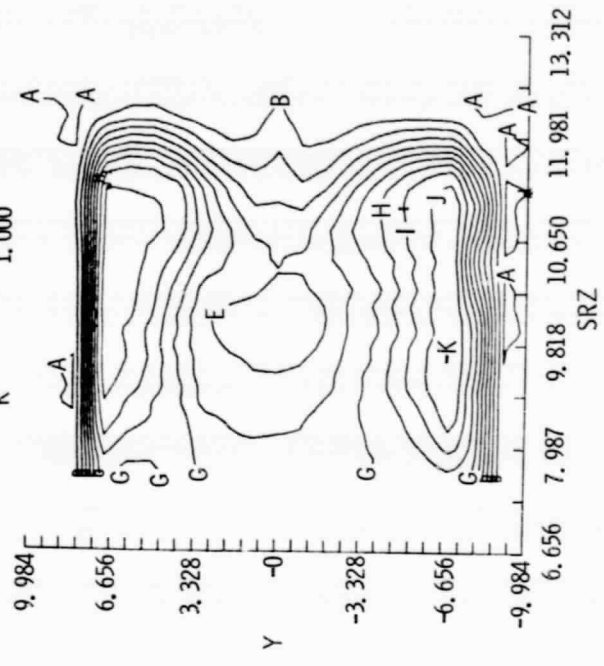
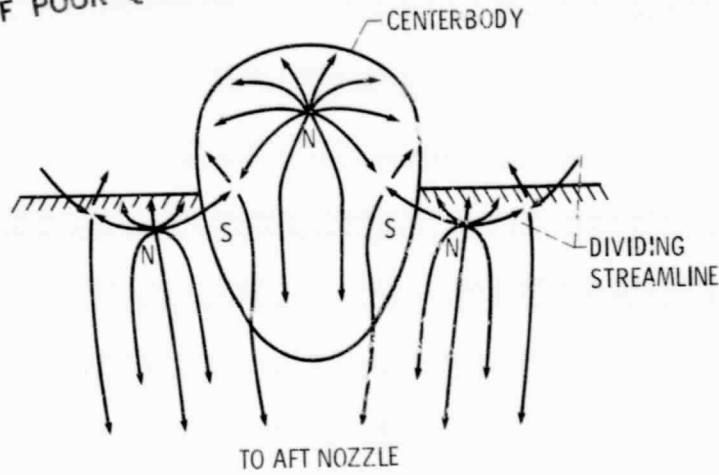


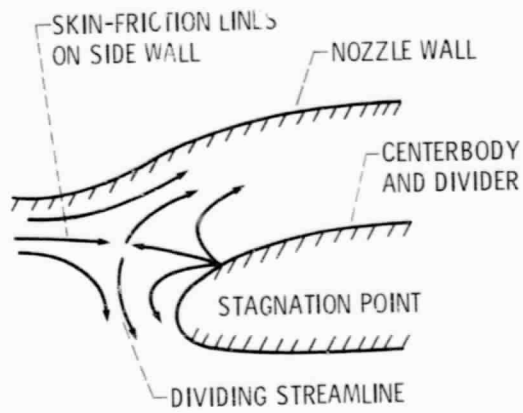
Figure 32. - Total pressure contours at front nozzle exit.

Figure 31. - Proposed skin-friction lines.

ORIGINAL PAGE IS
OF POOR QUALITY



(a) Proposed skin-friction lines on top side of centerbody and divider.



(b) Side view of dividing streamline.

Figure 33. - Interpretation of skin-friction lines.



Figure 34. - Streaks on aft nozzle wall.

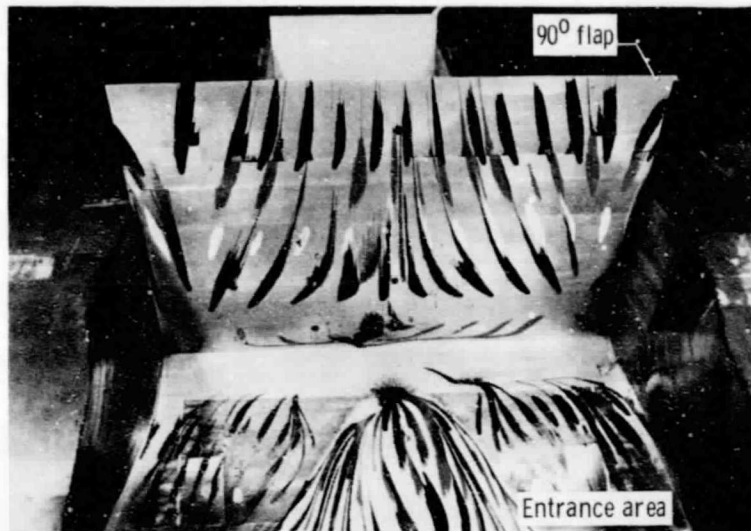


Figure 35. - Flow visualization of flap and underside of divider of front nozzle (installed inversely).

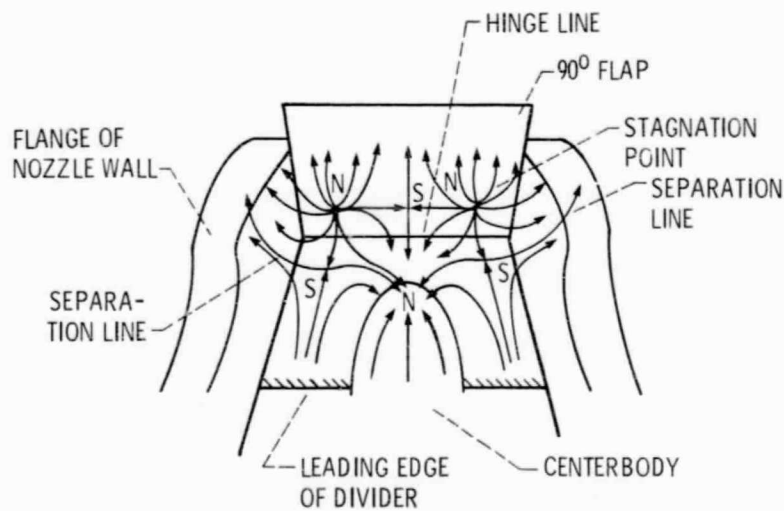


Figure 36. - Postulated skin-friction lines on flap and underside of divider of front nozzle.

ORIGINAL PAGE IS
OF POOR QUALITY

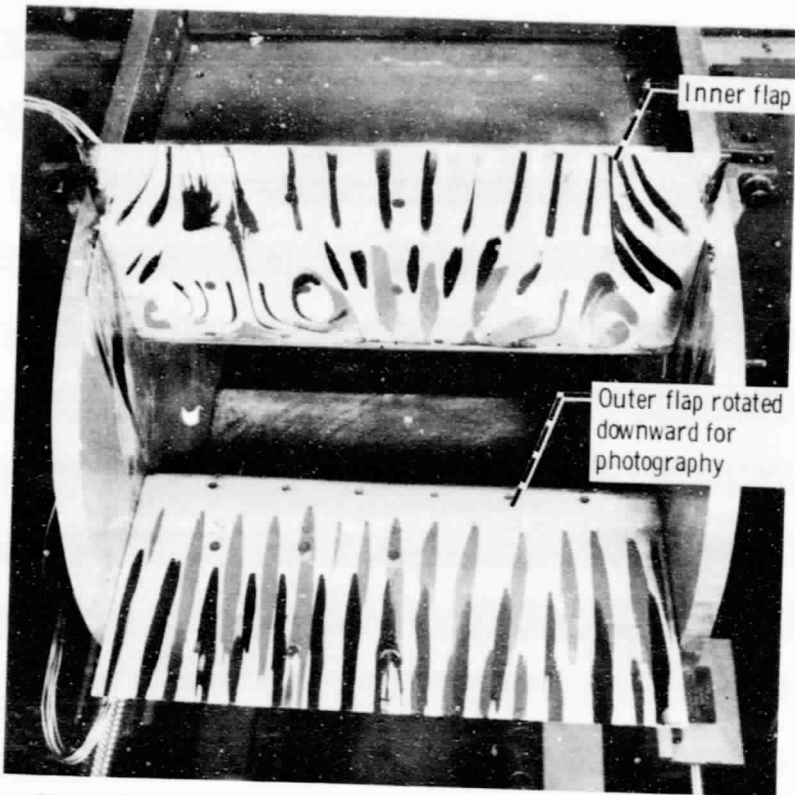


Figure 37. - Flow visualization at aft nozzle with both flaps at 90° .

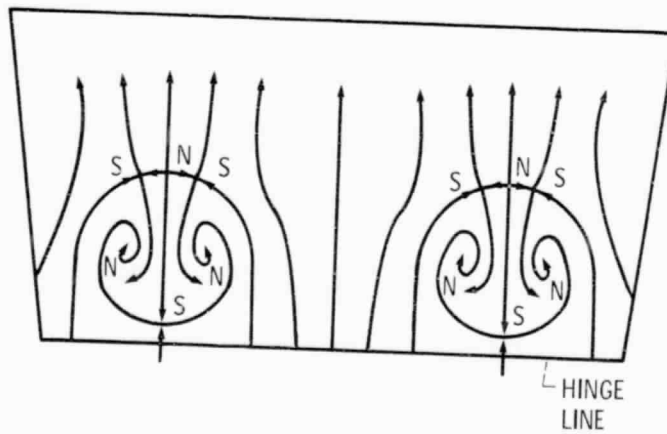


Figure 38. - Interpretation of skin-friction lines on inner flap of aft nozzle.

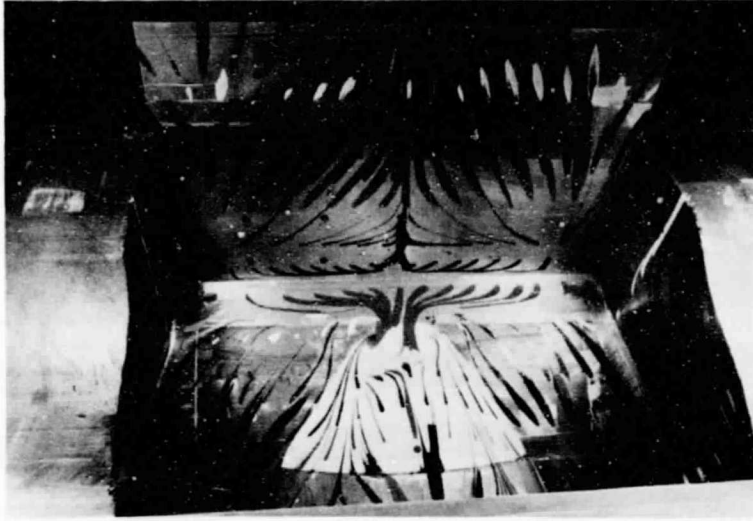
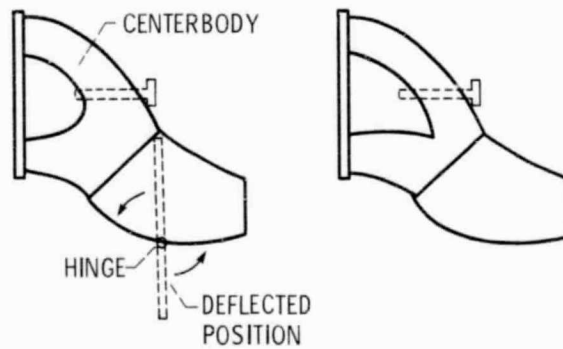


Figure 39. - Streaks on 90° flap and underside of divider with front nozzle alone open.



(a) Regular centerbody.

(b) Whale-tail.

Figure 40. - Tandem-fan front nozzle.

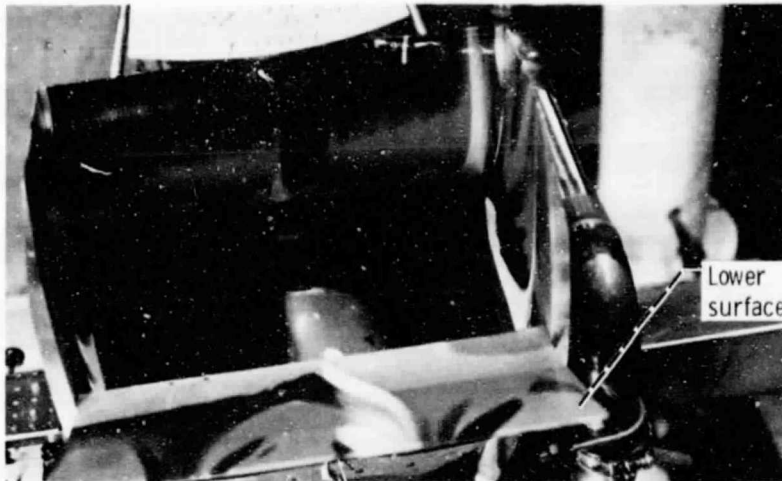


Figure 41. - Streaks on tandem-fan front nozzle with regular centerbody (installed inversely with lower surface rotated downward for photography).

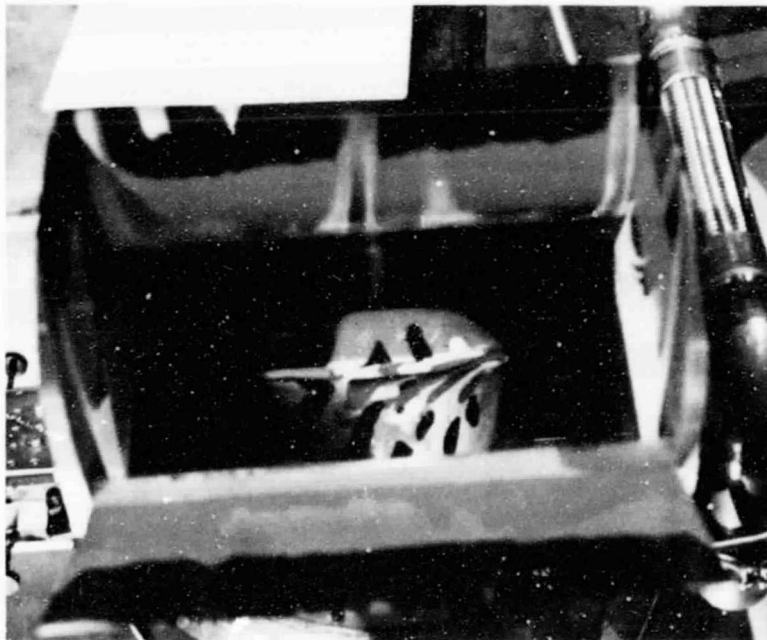
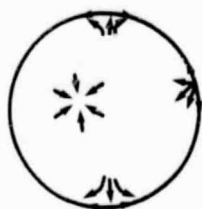
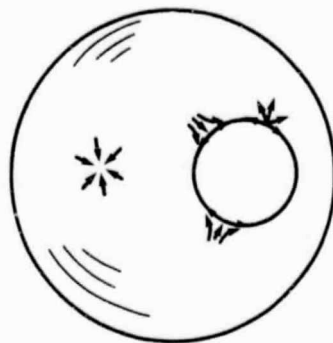


Figure 42. - Streaks on tandem-fan front nozzle with whale-tail centerbody (installed inversely with lower surface rotated downward for photography).

ORIGINAL PAGE IS
OF POOR QUALITY



(a) A disk with interior and boundary singular points.



(b) A sphere with a circular hole transformed from the disk in (a).

Figure A-1. - Graphical derivation of equation (3).